1

Self-Assembled Delivery Vehicles for Poorly Water-Soluble Drugs: Basic Theoretical Considerations and Modeling Concepts

Sylvio May and Alfred Fahr

1.1 Introduction

Poor solubility is a well-recognized property of many drug molecules [1]. Unprotected administration of poorly water-soluble drugs is problematic. Aggregation, precipitation, uncontrolled binding, and direct exposure to a harsh biological environment render this process inefficient. The putative 'solution' of using higher drug concentrations narrows the window between a therapeutic success and unwanted side effects such as locally toxic drug levels. It comes as no surprise that the administration of poorly water-soluble drugs can benefit dramatically from using delivery vehicles. Such vehicles can, in principle, be designed not only to encapsulate a drug and protect it from biological defense mechanisms, but also to release the drug in a controlled manner at the target site and then to be recycled through biodegradation. Different types of delivery vehicles are currently being investigated, including microemulsions [2, 3], gels [4], micelles [5, 6], liposomes [7], polymersomes [8], dendrimers [9], and nanopcrystals [10], or lipid nanoparticles [11]. Notably, most of these are self-assembled structures. Self-assembly is an ubiquitous process in cellular systems, most strikingly perhaps in the cell membrane where a matrix (lipids) contains highly specialized functional units (poorly water-soluble proteins). Functionalization is an advantage that is also increasingly integrated into drug delivery vehicles. As an example

Drug Delivery Strategies for Poorly Water-Soluble Drugs, First Edition. Edited by Dennis Douroumis and Alfred Fahr.

we mention liposomes, which were originally designed as long-circulating transport vehicles for drug molecules [12]. Extending the circulation time by decorating the liposome surface with PEG-chains (stealth liposomes [13]) can be viewed as the first step toward functionalization. Currently designed liposomes raise the concept of functionalization to a new height: they contain targeting ligands and carry out stimuli-sensitive triggering of the drug release [14–16].

Optimizing drug delivery vehicles is promising but also challenging. Self-assembled nanostructures are soft and responsive materials, where entropy becomes an important factor for structure and stability. It is virtually impossible to manipulate one property without affecting others (and sometimes this has drastic implications as one of the authors vividly recalls the disintegration of an entire colloidal formulation upon the replacement of a single -H group by an -OH group in a 1 kDalton drug molecule). Nanocarrier properties are affected by a range of interactions that are well known from colloidal science, including solvation energies, electrostatic and van der Waals interactions, depletion and packing effects, etc. [17, 18]. Appreciation and understanding of these interactions are likely to reflect upon nanocarrier design and optimization. For example, one of the challenges that drug encapsulation in nanocarriers faces is related to the retention of the drug in the carrier. A lipophilic drug does not necessarily remain in a *rigid* lipophilic matrix [19] but is rapidly squeezed out, whereas *soft* structures (like liposomal membranes) tend to increase the residence time in the membrane. What physical mechanisms underlie the ability of soft rather than rigid self-assembled structures to accommodate small lipophilic drugs? And what physical properties determine the release? The latter question relates to the fact that a carrier keeping the drug completely in the interior will ultimately prevent a therapeutic effect. The authors' experience with a liposomal formulation of a peptide showed an increase of lifetime from 3 mins to 24 hours in blood, but there was no pharmacological activity, as the liposomes with the drug inside were eliminated without releasing the drug to blood components or organs. Other practical hurdles are discussed, for example, by van Hoogevest *et al*. [20].

The present chapter presents a conceptual framework for physics-based modeling approaches of self-assembled nanoscaled carrier systems that are associated with lipophilic drugs. Our focus is clearly on the basic physics and underlying concepts [21]. We start with an account of basic thermodynamic relations (Section 1.2) which we subsequently exploit to discuss principles of self-assembly (Section 1.3) and the partitioning of drug molecules into self-assembled carrier systems (Section 1.4). The energetics of individual delivery vehicles depends on a multitude of inter-molecular interactions; of these we discuss electrostatics and the packing of chain-like molecules (Section 1.5). We finally consider kinetic properties of drug transfer from mobile nano-carriers to a target system (Section 1.6). Note that none of the sections aims to give a comprehensive account of the available theoretical concepts (for more comprehensive accounts and discussions of specific applications, see [21–24]). However, for those subjects that we discuss, it is our goal not only to state the final results but also provide some guidance through the physical and mathematical basis of their derivation. We shall focus on simple and generic models, namely those that highlight the underlying physical principles, thereby excluding more advanced theoretical concepts and atomistic simulations. In summary, the present chapter approaches the pharmaceutical scientist who is interested in the process of developing theoretical models for self-assembled delivery vehicles of drug molecules from first principles.

1.2 Brief Reminder of Equilibrium Thermodynamics

We start by briefly recalling some basic concepts of equilibrium thermodynamics and statistical mechanics, thereby focusing on those aspects that will become important in the subsequent parts of this chapter. For each thermodynamic system there exists a thermodynamic potential F that contains all thermodynamic information. This means it encodes for all thermodynamic equations of state (such as the van der Waals equation of state for a van der Waals fluid, etc.). The potential F depends on a number of degrees of freedom that the system possesses. Some of these degrees of freedom can adjust only slowly; they are referred to as constrained variables. The remaining degrees of freedom correspond to unconstrained variables: they can adjust quickly. Equilibrium thermodynamics can only be applied if there exists a time window that separates the constrained from the unconstrained variables. (Note that this statement is very different from the demand of true thermal equilibrium.) Equilibrium thermodynamics – like most other fundamental physical theories – can be formulated as a minimization principle: The thermodynamic potential F adopts its minimum state with respect to all unconstrained variables. This eliminates the unconstrained variables from F. We note that statistical mechanics performs the very same minimization, yet starting from a representation of the potential F that includes all relevant microscopic degrees of freedom. In this entire chapter we treat the temperature T as a fixed constant. The thermodynamic potential – referred to as Helmholtz free energy – can then be expressed as $F = U - TS$ where U and S are the internal energy and entropy of the system under consideration. The free energy $F = U - TS$ can be viewed as a Legendre transformation from given entropy to fixing the temperature of the system by adding a heat bath of temperature T.

It is instructive to actually perform the minimization of F with respect to all its unconstrained variables. To this end, we consider a system that can exist in many different states α. To be specific, the different states α could refer to different spatial arrangements of surfactants and drug molecules that form a mixed surfactant micelle. This is schematically illustrated in Figure 1.1. Obviously, there are many different arrangements of the drug molecules and corresponding conformations of the micelle – so the total number of states may be extremely large. Each state α will be adopted with a probability $P(\alpha)$. These probabilities are normalized according to $\sum_\alpha P(\alpha) = 1$. If each state has an internal energy $u(\alpha)$, we can write the total internal energy as $U = \sum_\alpha u(\alpha)P(\alpha)$.

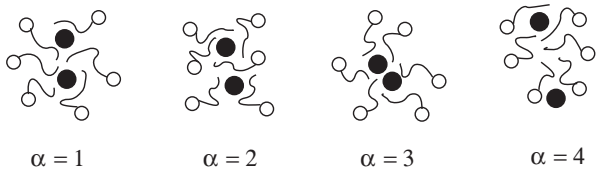

Figure 1.1 *Schematic illustration of a micelle, formed by six single-chained surfactants and two drug molecules (filled circles). Four arbitrarily chosen states α (out of a very large number of possible states) are displayed. Real surfactant micelles are typically composed of 50 to several hundred individual molecules and can contain some tens to 200 of drug molecules [25].*

The entropy can be expressed as a function of $P(\alpha)$ only: $S = -k_B \sum_\alpha P(\alpha) \ln P(\alpha)$. Here, $k_B = 1.38 \times 10^{-23} J/K$ is the Boltzmann constant. We note that only the form $P \ln P$ translates a multiplicativity of the probabilities into an additivity of the entropies; hence, this form of the entropy ensures extensivity of S. The thermodynamic potential thus reads $F = U - TS = \sum_\alpha P(\alpha)[u(\alpha) + k_B T \ln P(\alpha)]$. Clearly, the probabilities $P(\alpha)$ are not constrained; so they correspond to the set of unconstrained degrees of freedom for the present system. Hence, F must adopt a minimum subject to $P(\alpha)$. From the minimization of F we obtain the equilibrium distribution $P(\alpha) = \exp[-u(\alpha)/k_B T]/Q$ where $Q = \sum_\alpha \exp[-u(\alpha)/k_B T]$ ensures proper normalization as stated above. The distribution of probabilities for the different states α is the familiar Boltzmann distribution, and Q is referred to as the partition sum. The partition sum plays a central role as can be seen upon inserting the Boltzmann distribution back into F, yielding $F = -k_B T \ln Q$. Hence calculating Q gives immediate access to the thermodynamic potential F.

As a specific example we consider a fluid that has all its particles (i.e., molecules) confined to the sites of a lattice (this is also known as a lattice gas [26]). The lattice gas is certainly oversimplified but it serves as an instructive model, particularly for a binary fluid with roughly equal-sized solute and solvent molecules. Assume the lattice consists of M sites total; N sites are occupied by solute molecules and $M - N$ sites host solvent molecules. Figure 1.2(a) shows the lattice model. The dimensionality and connectivity of the lattice are irrelevant as long as the molecules do not interact with each other. In this case, the partition sum simply corresponds to the number $Q = M!/[N!(M - N)!]$ of available arrangements of the solute and solvent molecules. The use of Stirling's approximation $\ln x! \approx x \ln x - x$ (which is valid for $x \gg 1$) leads to the thermodynamic potential $F = -k_B T \ln Q = k_B T M[\phi \ln \phi + (1 - \phi) \ln(1 - \phi)]$ where we have defined the mole fraction

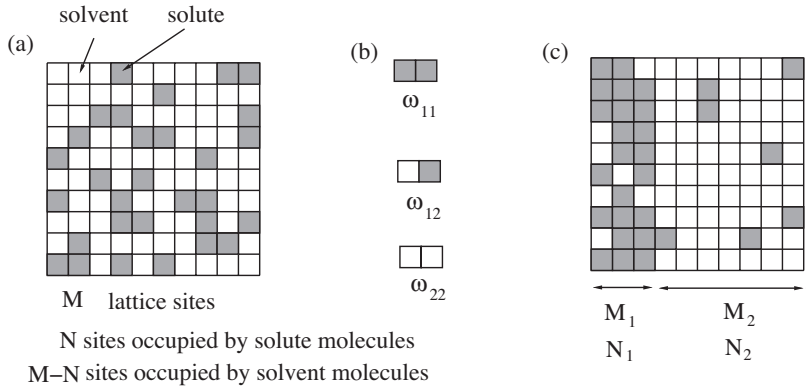

Figure 1.2 (a) *Schematic illustration of the lattice model. A two-dimensional square lattice of* $M = 100$ *lattice sites is shown, it contains* $N = 30$ *solute molecules and* $M - N = 70$ *solvent molecules.* (b) *Inter-molecular interactions can be characterized by a solute-solute* (ω_{11})*, solute-solvent* (ω_{12})*, and solvent-solvent* (ω_{22}) *interaction strength.* (c) *For sufficiently strong interactions the system may phase separate into a solute-rich phase (with* N_1 *solute molecules in a sublattice of* M_1 *sites), and a solute-poor phase (with* $N_2 = N - N_1$ *solute molecules in a sublattice of* $M_2 = M - M_1$ *sites). Note that* M_1, M_2, N_1, N_2 *are determined by the common tangent construction; see Equation 1.2.*

$\phi = N/M$ of solute molecules. Dissolving the solute in the solvent leads to a decrease in F which, in principle, can be used as work. This available (free) energy is entirely of entropic origin (i.e., $U = 0$ in $F = U - TS$). We note that for small solute mole fraction, $\phi \ll 1$, the free energy $F = k_B T M \phi(\ln \phi - 1)$ is identical to the free energy of an ideal gas. In fact, for *any* mixed system sufficient dilution leads to an ideal gas.

Let us go one step further and introduce interactions between the molecules. We will do this only on the so-called mean-field level, where correlations are ignored [26]. (Roughly speaking, in mean-field theory the interactions of a given particle are approximated by an effective interaction that only accounts for the net effect but not the details of the environment.) To this end, we consider a lattice of coordination number z. The coordination number simply denotes the number of next neighbors of each given lattice site, i.e., $z = 4$ for the two-dimensional square lattice illustrated in Figure 1.2(a), etc. Denote the (nearest-neighbor) solute-solute, solute-solvent, and solvent-solvent interaction strengths by ω_{11}, ω_{12}, and ω_{22}; see Figure 1.2(b). Neglecting correlations amounts to a random mixing approximation [26] where the total internal energy of the system is $U = Mz[\omega_{11}\phi^2 + 2\omega_{12}\phi(1-\phi) + \omega_{22}(1-\phi)^2 - \phi\omega_{11} - (1-\phi)\omega_{22}]/2$. The first three terms account for the solute-solute, solute-solvent, and solvent-solvent interactions, and the last two terms subtract the fully demixed reference state, one for the solute and the other for the solvent. The total internal energy per lattice site, $U/M = \chi\phi(1-\phi)$, can thus be expressed in terms of a single effective interaction parameter $\chi = z[\omega_{12} - (\omega_{11} + \omega_{22})/2]$, also referred to as the non-ideality parameter. Note that the non-ideality parameter is positive if molecules of the same type effectively attract each other, $(\omega_{11} + \omega_{22})/2 < \omega_{12}$. Based on the interaction term U and the ideal mixing free energy $-TS$, the overall free energy $F = U - TS$ of the interacting lattice gas can be expressed as $F = Mf$ where the free energy per lattice site is

$$f = \chi\phi(1-\phi) + k_B T\,[\phi \ln \phi + (1-\phi)\ln(1-\phi)]\,. \tag{1.1}$$

The left diagram of Figure 1.3 displays $f = f(\phi)$ for different choices of χ. For sufficiently large χ the curves exhibit a concave region, centered about $\phi = 0.5$. Concavity of $f(\phi)$ is of thermodynamic significance as it implies that the system is *locally* unstable. To explain this instability we consider two equal-sized sublattices with initially the same composition ϕ. If a small number of solute molecules migrate from one to the other sublattice, the total free energy decreases given that the free energy $f(\phi)$ is concave. Mathematically this instability can be expressed as $f(\phi + \triangle\phi) + f(\phi - \triangle\phi) < 2f(\phi)$ for small $\triangle\phi$, or, equivalently, as $f''(\phi) < 0$, where the prime denotes the derivative with respect to the argument ($f'(\phi) = df/d\phi$, etc). Regions with $f''(\phi) > 0$ are locally stable, and regions with $f''(\phi) < 0$ are locally unstable. They are separated by points of inflection where $f''(\phi) = 0$. The points of inflection are marked in Figure 1.3(a) by the symbol $\diamond$ for the curve corresponding to $\chi = 3\,k_B T$). For Equation 1.1 the condition $f''(\phi) < 0$ translates into $k_B T/\chi < 2\phi(1-\phi)$. Concavity is a sufficient but not a necessary condition for thermodynamic instability to occur. A more general condition can be derived by considering two different phases (one of size M_1 with N_1 solute molecules and the other of size $M_2 = M - M_1$ with $N_2 = N - N_1$ solute molecules) with corresponding free energy $F = M_1 f(\phi_1) + (M - M_1) f(\phi_2)$ where $\phi_1 = N_1/M_1$ and $\phi_2 = (N - N_1)/(M - M_1)$ are the mole fractions of solute molecules in the two phases. A lattice that contains two different phases is illustrated in Figure 1.2(c). If the two phases are indeed thermodynamically stable, they must represent a minimum

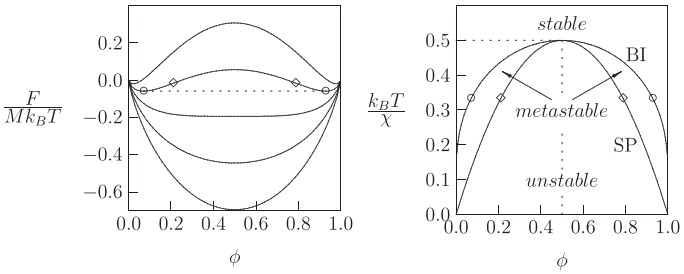

Figure 1.3 Left diagram: *Free energy per lattice site $F/(Mk_BT) = f/k_BT$ according to Equation 1.1 for different choices of the non-ideality parameter, $\chi/k_BT = 0, 1, 2, 3, 4$ (from bottom to top). For $\chi/k_BT = 3$, the points of inflection and the points that give rise to a common tangent are marked by the symbols $\diamond$ and $\circ$, respectively. The common tangent is indicated by the dotted line.* Right diagram: *Phase diagram k_BT/χ versus ϕ, with the spinodal (SP) and binodal (BI) lines indicated. Upon increasing the temperature T the system generally passes from a locally unstable region via a metastable region to a stable single phase system. It thereby crosses first the spinodal and then the binodal line. The symbols $\diamond$ and $\circ$ in the left diagram correspond to the ones in the right diagram (i.e., for $\chi/k_BT = 3$). The dotted lines in the right diagram indicate the critical point $\chi_c/k_BT = 2$ and $\phi_c = 1/2$.*

of F with respect to the two unconstrained parameters N_1 and M_1. This implies the two equations $\partial F/\partial N_1 = f'(\phi_1) - f'(\phi_2) = 0$ and $\partial F/\partial M_1 = f(\phi_1) - f(\phi_2) - \phi_1 f'(\phi_1) + \phi_2 f'(\phi_2) = 0$, giving rise to the common tangent construction [27]

$$f'(\phi_1) = f'(\phi_2) = \frac{f(\phi_2) - f(\phi_1)}{\phi_2 - \phi_1} \tag{1.2}$$

for the two coexisting compositions ϕ_1 and ϕ_2. As long as the system contains coexisting phases, the free energy moves along the common tangent, thus ensuring that the adopted thermodynamic potential does not become concave. The common tangent, which marks the region of global instability, is indicated in the left diagram of Figure 1.3 for the curve corresponding to $\chi = 3\,k_BT$ (see the dotted line between the two $\circ$ symbols). The regions of local and global instability can be mapped into a phase diagram k_BT/χ versus ϕ; see the right diagram of Figure 1.3. The lines separating regions of local and global instability are called spinodal (SP) and binodal (BI), respectively. The region between the spinodal and binodal is metastable. Here, the system can reside in a homogeneous single-phase state or phase separate (which lowers the free energy below that of the single-phase state). The largest k_BT/χ where phase separation occurs is the critical point; that point can generally be found by solving the two equations $f''(\phi) = f'''(\phi) = 0$ with respect to χ and ϕ. For Equation 1.1, this yields the critical point $\chi = \chi_c = 2k_BT$ and corresponding critical composition $\phi = \phi_c = 1/2$.

We note that the free energy in Equation 1.1 is based on a simple lattice model which despite being too simplistic to quantitatively describe real systems captures the principal features that lead to a phase transition. There are plenty of other, more elaborate and realistic, free energy expressions that predict phase diagrams (and corresponding critical points) using the same formalism that yields the phase diagram in Figure 1.3. For example,

the van der Waals fluid has a free energy, expressed per lattice site (of unit volume) of $f = a\phi^2 + k_BT\phi\ln[\phi/(1-b\phi)]$. The two material parameters a and b describe the degree of intermolecular attraction and the molecular eigenvolume; ϕ is the mole fraction of the solute as above. Calculation of the pressure

$$P = -\frac{d[f(\phi)/\phi]}{d(1/\phi)} = \phi\frac{df}{d\phi} - f = \frac{\phi k_BT}{1-b\phi} + a\phi^2 \tag{1.3}$$

yields the familiar van der Waals equation of state [26]. Upon solving the two equations $f''(\phi) = f'''(\phi) = 0$ we obtain the critical point of the van der Waals fluid, $a = -27b\,k_BT/8$ and $\phi = 1/(3b)$. The mean-field lattice gas model leading to Equation 1.1 can also be extended to a polymer/solvent mixture. Here, the solute (i.e., the polymer) is represented by n (connected) segments, each occupying a single lattice site. Denoting the volume fraction of the polymer by ϕ, the (mean-field) free energy per lattice site becomes

$$f = \chi\phi(1-\phi) + k_BT\left[\phi\ln\phi + \frac{1}{n}(1-\phi)\ln(1-\phi)\right], \tag{1.4}$$

where χ/k_BT is known as the Flory-Huggins parameter that describes the effective polymer segment-solvent interaction strength [28]. The segment number n has a profound influence on the phase behavior as can be seen from the critical point $\chi_c = (1+1/\sqrt{n})^2\,k_BT/2$ and $\phi_c = 1/(1+\sqrt{n})$. Large n (10^3 is a typical value) drives phase separation already at polymer volume fractions of only a few percent. Flory-Huggins parameters for drug-polymer systems can either be extracted from experiments [29] or predicted via computer simulations [30].

1.3 Principles of Self-Assembly in Dilute Solutions

Self-assembly is a fundamental process with relevance for many of the delivery vehicles that are being used to deliver poorly water-soluble drugs [31]. Among the most relevant examples are micellar structures that are composed of surfactants, lipids, or polymers [24, 32]. Yet, self-assembly is also encountered for hydrophobic drug molecules, such as photosensitizers, when dissolved in an aqueous environment [33]. In this case, the aggregation state can be modulated by adding additional drug-binding proteins [34].

In this section we review the thermodynamic principles behind self-assembly processes [35, 36]. Rather than merely stating the results we aim to make the thermodynamic origin of the principles transparent. We focus on dilute solutions where a number of N chemically identical solute molecules are able to form N_i aggregates of aggregation number i. That is, N_1 is the number of monomers, N_2 the number of dimers, etc. This is illustrated for a specific example in Figure 1.4. As in the previous section, we adopt a lattice description of the system where a solvent molecule and a solute molecule each occupy one single lattice site. The N solute molecules thus self-assemble on a lattice of M sites. Note that using a lattice is convenient and does not limit the generality of the model in the dilute limit (as it did not for the ideal gas). The total volume of the system is then $V = M\nu$, where ν denotes the volume per lattice site. Dilute conditions require $N \ll M$. Here, the system can be

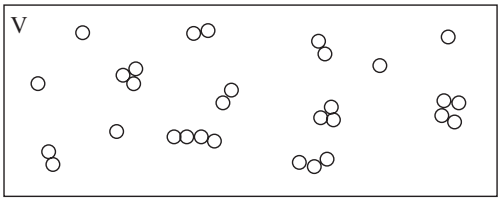

Figure 1.4 *Schematic illustration of $N = 30$ solute molecules (each represented by the symbol ○) that – in this particular snapshot – self-assemble into $N_1 = 5$ monomers, $N_2 = 4$ dimers, $N_3 = 3$ tri-mers, and $N_4 = 2$ four-mers. Note that $\sum_i i N_i = N$.*

described as a mixed ideal gas, where each component is represented by the corresponding N_i aggregates of aggregation number i. The free energy of the system

$$F = \sum_{i=1}^{N} \left[N_i \mu_i^0 + k_B T N_i \left(\ln \frac{N_i}{M} - 1 \right) \right] \tag{1.5}$$

is then simply the sum of the individual ideal gas free energies, each with its own standard chemical potential μ_i^0 per i-mer. The sum runs from $i = 1$ (monomers) to $i = N$ where all solute molecules form one single aggregate. The limit $i = N$ can be relevant. Lipid bilayers, for example, tend to fuse, despite the loss of translational entropy upon the merger of two bilayers into one. We note that the conservation of the total number of solute molecules implies $\sum_{i=1}^{N} i N_i = N$. In the following it is convenient to use the mole fractions $\phi_i = i N_i / M$ of solute molecules that form i-mers. Similarly, we introduce the total mole fraction of solute molecules $\phi = N/M$ in the system. The free energy in Equation 1.5, expressed per lattice site, then reads

$$f = \frac{F}{M} = \sum_{i=1}^{N} \left[\phi_i \tilde{\mu}_i^0 + k_B T \frac{\phi_i}{i} \left(\ln \frac{\phi_i}{i} - 1 \right) \right], \tag{1.6}$$

where we have introduced the standard chemical potential $\tilde{\mu}_i^0 = \mu_i^0 / i$ per solute molecule in an i-mer. The distribution ϕ_i constitutes a set of unconstrained degrees of freedom (similar to the probabilities $P(\alpha)$ in the preceding sub-section). Yet, the minimization of f with respect to the ϕ_is must account for the additional conservation $\sum_{i=1}^{N} \phi_i = \phi$ of the total number of solute molecules. A minimization subject to an additional constraint is a problem that occurs frequently in science and for which mathematics offers the method of introducing a so-called Lagrange multiplier [37]. Let us illustrate its use. We define the auxiliary function $\tilde{f} = f - \mu \sum_{i=1}^{N} \phi_i$ which introduces the Lagrange multiplier μ. Note that μ is unspecified as of now but can be determined later so that the additional constraint $\sum_{i=1}^{N} \phi_i = \phi$ becomes satisfied. The introduction of μ allows us to minimize $\tilde{f}$ with respect to *all* ϕ_i. From $\partial \tilde{f} / \partial \phi_i = 0$ we find the equilibrium distribution $\phi_i = i \exp[-(\tilde{\mu}_i^0 - \mu)/k_B T]$. The role of the Lagrange multiplier μ becomes transparent after calculating the chemical potential $\mu_i = \partial F / \partial (i N_i) = \partial f / \partial \phi_i = \tilde{\mu}_i^0 + (k_B T / i) \ln(\phi_i / i)$ of a solute molecule that resides in an i-mer. Comparing this with the equilibrium distribution $\mu = \tilde{\mu}_i^0 + (k_B T / i) \ln(\phi_i / i)$, we conclude $\mu_i = \mu$ for *all* i-mers. Hence, in equilibrium all solute molecules have

the same chemical potential, and that chemical potential is equal to the Lagrange multiplier μ. We proceed with two more remarks. First, the relation $\mu_1 = \mu_i$ can be expressed [17] as

$$\frac{(N_i/M)}{(N_1/M)^i} = \frac{\phi_i/i}{\phi_1^i} = e^{-i(\tilde{\mu}_i^0 - \tilde{\mu}_1^0)/k_BT} = K_i. \tag{1.7}$$

This can be interpreted as the familiar mass action law for the association reaction $i\,\mathrm{A} \overset{K_i}{\rightleftharpoons} \mathrm{A}_i$, where i monomers form one single i-mer; K_i is the corresponding equilibrium constant, and $i(\tilde{\mu}_i^0 - \tilde{\mu}_1^0)$ is the standard change in free energy for the association event. Note that the association reaction does not imply that an i-mer actually forms from i monomers; that process may take a different route such as adding a single monomer and an $(i-1)$-mer. Second, inserting the equilibrium distribution ϕ_i back into the free energy yields, $f = \mu\phi - k_BT\sum_{i=1}^{N}\phi_i/i$. This can be interpreted as the familiar thermodynamic relation for the Helmholtz free energy $F = G - PV$ in terms of the Gibbs free energy $G = \mu N$ and the pressure $P = (\partial F/\partial V)_T$ (where we recall $V = Mv$). Further analysis of the aggregation behavior requires the specification of the function $\tilde{\mu}_i$. We consider two cases of principal importance: linear growth and cooperative assembly.

1.3.1 Linear Growth

Here aggregates can grow along one dimension only as is the case for biological filaments or worm-like micelles. Each monomer within the aggregate contributes the same (namely μ_b) to the standard chemical potential $\mu_i^0 = i\tilde{\mu}_i^0$ per aggregate. Only the two terminal segments each add an additional contribution $\delta/2$; see the illustration at the top of Figure 1.5. The model for linear growth can thus be written as $\mu_i^0 = i\mu_b + \delta$. It is the excess terminal

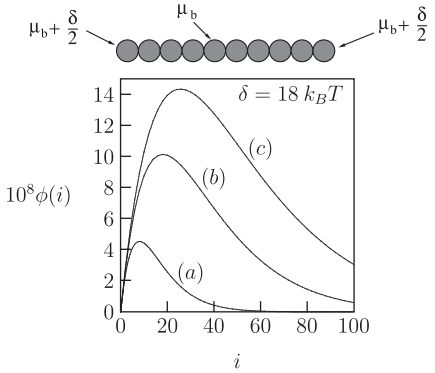

Figure 1.5 *Plot of $\phi(i)$ according to Equation 1.8. The excess contribution to the standard chemical potential is $\delta = 18k_BT$ for all curves. The total mole fraction of the solute is $\phi = 10^{-6}$ (a), $\phi = 5\times10^{-6}$ (b), and $\phi = 10^{-5}$ (c). Note that for each curve the relation $\int_0^\infty \phi(i)\,di = \phi$ is fulfilled. The top of the diagram shows an illustration of a 10-mer, i.e., a linear aggregate with $i = 10$. Here, μ_b is the standard chemical potential per monomer in the bulk of the aggregate. The two terminal segments each make an additional (i.e., excess) contribution $\delta/2$ to the standard chemical potential $\mu_i^0 = i\mu_b + \delta$.*

contribution δ that is gained when two linear aggregates combine into a single one. This gain drives the growth into fewer and longer aggregates, despite the larger entropy that many small aggregates would have. Note that a monomeric unit need not necessarily be identified with a single solute molecule. For example, when modeling worm-like micelles it is convenient to identify a single spherical micelle with a monomeric unit [36]. Upon initiating growth these micelles dynamically combine into elongated (i.e., linearly extended) structures.

Let us investigate the thermodynamics behind self-assembled linear structures. To simplify the calculation we assume $\delta \gg k_B T$ for which the aggregates grow very long so that we can treat $\phi_i \to \phi(i)$ as a function of the continuous variable i and approximate the summation by an integration, $\sum_{i=1}^{N} \to \int_0^\infty di$. From the normalization condition $\phi = \int_0^\infty \phi(i) di$ we then find the chemical potential $\mu = \mu_b - k_B T e^{-\delta/(2k_B T)}/\sqrt{\phi}$. Inserting this into the distribution $\phi(i)$ yields

$$\phi(i) = i \exp\left[-\frac{\delta}{k_B T} - \frac{i}{\sqrt{\phi}}\, e^{-\frac{\delta}{2k_B T}}\right]. \tag{1.8}$$

This distribution adopts a maximum at the aggregation number $i = i_m$ with $i_m = \sqrt{\phi}\, e^{\delta/(2k_B T)}$. To further characterize the distribution, we define the weight-average $\langle Q \rangle = \int_0^\infty \phi(i)\, Q(i)\, di / \int_0^\infty \phi(i)\, di$ of any physical quantity $Q = Q(i)$. The weight average of the size distribution is then $\langle i \rangle = 2i_m$. Similarly, for the standard deviation of the size distribution we obtain $\sigma = \sqrt{\langle (i - \langle i \rangle)^2 \rangle} = \sqrt{2}\, i_m$.

Hence, we conclude that the linear growth model leads to a broad equilibrium distribution of aggregate lengths, where the standard deviation of the sizes $\sigma = \langle i \rangle/\sqrt{2}$ is about 70% of the average size distribution $\langle i \rangle$. In Figure 1.5 we display $\phi(i)$ for some examples (all with $\delta = 18 k_B T$ but different choices of ϕ). Since μ and $\phi(i)$ are known, we can explicitly calculate the Helmholtz free energy F of the system; this leads to

$$F = N\left[\mu_b - \frac{2k_B T}{\sqrt{\phi}}\, e^{-\frac{\delta}{2k_B T}}\right]. \tag{1.9}$$

For small T all solute molecules assemble into one single aggregate, implying $F = N\mu_b$.

1.3.2 Cooperative Assembly

The second principal scenario that we discuss is when a certain number of solute molecules must come together to form a single aggregate. This is the case, for example, when surfactants start forming micelles or when peptides cooperatively form a pore in a lipid membrane. While the number of surfactants in micelles can certainly vary, we only consider the most simple scenario, where exactly n solute molecules form one single aggregate. To exclude all other aggregation numbers, we chose $\tilde{\mu}_i^0 \to \infty$ (implying $\phi_i = 0$) for all i unless $i = 1$ or $i = n$. The distribution of the remaining monomers and n-mers is then specified by $\phi_1 = e^{-(\tilde{\mu}_1^0 - \mu)/k_B T}$ and $\phi_n = e^{-n(\tilde{\mu}_n^0 - \mu)/k_B T}$, subject to $\phi_1 + \phi_n = \phi$. We thus have three equations for the three unknown quantities ϕ_1, ϕ_n, and μ. These equations can be solved numerically. In Figure 1.6 we show $\phi_1(\phi)$ and $\phi_n(\phi)$ for the two different choices $n = 10$ and $n \to \infty$, both at fixed $\tilde{\mu}_1^0 - \tilde{\mu}_n^0 = 5 k_B T$. The limiting behavior for $n \to \infty$ is given by $\phi_1 = \phi$ and $\phi_n = 0$ for $\phi < \phi_{cmc}$, as well as $\phi_1 = \phi_{cmc}$ and $\phi_n = \phi - \phi_{cmc}$ for $\phi > \phi_{cmc}$. The critical value ϕ_{cmc} reflects the so-called critical micelle concentration

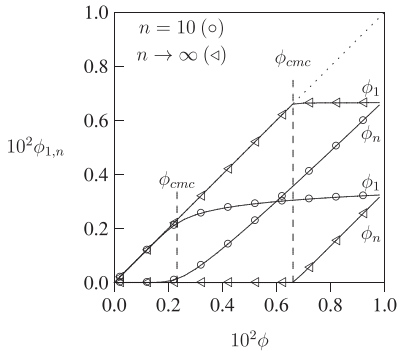

Figure 1.6 *The mole fractions ϕ_1 and ϕ_n as function of the total mole fraction ϕ for cooperative assembly with $n = 10$ (curves marked by the symbol ○) and $n \to \infty$ (marked by the symbol ◁), both calculated for $\tilde{\mu}_1^0 - \tilde{\mu}_n^0 = 5k_BT$. The corresponding two critical mole fractions ϕ_{cmc} are indicated by the vertical broken lines. Note $\exp[-(\tilde{\mu}_1^0 - \tilde{\mu}_n^0)/k_BT] = 0.673 \times 10^{-2}$; see Equation 1.10. The dotted line marks the total solute mole fraction $\phi = \phi_1 + \phi_n$.*

(CMC). A general definition (one that does not require large n) for ϕ_{cmc} simply identifies the point where 50% of the newly added solute molecules are used to form aggregates (whereas the other 50% remain as monomers) [18]. This can be expressed as $(d\phi_1/d\phi)_{\phi_{cmc}} = 1/2$. Evaluating this expression leads to

$$\phi_{cmc} = (1+n)\, n^{\frac{1+n}{1-n}} \exp\left[-\left(\frac{n}{n-1}\right)\left(\frac{\tilde{\mu}_1^0 - \tilde{\mu}_n^0}{k_BT}\right)\right] \approx \exp\left(-\frac{\tilde{\mu}_1^0 - \tilde{\mu}_n^0}{k_BT}\right), \quad (1.10)$$

where the approximate expression on the right-hand side of Equation 1.10 corresponds to the limit $n \to \infty$. Hence, the CMC can be used to extract the standard free energy of formation $\tilde{\mu}_1^0 - \tilde{\mu}_n^0 = -k_BT \ln \phi_{cmc}$. Finite values of n (see Figure 1.6 for $n = 10$) lead to a smeared-out transition at somewhat smaller ϕ_{cmc} than for $n \to \infty$.

1.4 Solubility and Partitioning of Drugs

1.4.1 Simple Partitioning Equilibria

The basis of designing delivery vehicles for poorly water-soluble drugs is their much higher solubility in apolar solvents as compared to water. We can characterize the thermodynamic partitioning of a solute between two strongly immiscible fluids most simply in the dilute limit. Here, the solute can be treated in each phase as an ideal gas, with corresponding free energy, $F = k_BTN(\ln\phi - 1) + N\mu^0$ where $\phi = N/M$ is the mole fraction of the solute (i.e., N solute molecules are dissolved in a phase that contains M solvent molecules). The chemical potential of the solute is $\mu = dF/dN = \mu^0 + k_BT \ln\phi$. Indexing the two phases '1' and '2', and setting the chemical potentials in the two phases equal, $\mu_1 = \mu_2$, leads to $\phi_2/\phi_1 = \exp[-(\mu_2^0 - \mu_1^0)/k_BT] = K^*$ where K^* is the partition coefficient. Hence, $-k_BT \ln(\phi_2/\phi_1) = \mu_2^0 - \mu_1^0$ directly yields the difference in the standard chemical potential of the solute in the two phases.

As the concentrations grow, deviations from ideal behavior become important. In this case, an activity coefficient $\gamma = \gamma(\phi)$ can be introduced into the expression for the chemical potential through $\mu = \mu^0 + k_B T \ln(\gamma\phi)$. Hence, the partition coefficient

$$K = \frac{\phi_2}{\phi_1} = \frac{\gamma_1}{\gamma_2}\, e^{-(\mu_2^0 - \mu_1^0)/k_B T} = \frac{\gamma_1(\phi)}{\gamma_2(\phi)}\, K^* \tag{1.11}$$

now depends on the activity coefficients and thus on the mole fractions of the solute in the two phases. Let us discuss a very simple but illustrative example that is based on the lattice model and corresponding mean-field free energy as introduced in Equation 1.1. Specifically, we consider two separated phases corresponding to M_1 and M_2 lattice sites, filled with two different solvents and, respectively, N_1 and N_2 identical solute molecules. The two phases may be immiscible or may be separated by a semi-permeable barrier (permeable only for the solute). For simplicity we assume $M_1 = M_2 = M/2$ so that the overall mole fraction of the solute becomes $\phi = (N_1 + N_2)/(M_1 + M_2) = (\phi_1 + \phi_2)/2$, where $\phi_1 = N_1/M_1$ and $\phi_2 = N_2/M_2$ are the mole fractions of the solute in the two phases. Let phase '1' be dilute and phase '2' be concentrated. The free energy $f_1 = k_B T \phi_1(\ln\phi_1 - 1) + \mu_1^0 \phi_1$ of the dilute phase can be treated as that of an ideal gas. According to Equation 1.1, we express the free energy of the concentrated phase as $f_2 = k_B T[\phi_2 \ln\phi_2 + (1 - \phi_2)\ln(1 - \phi_2)] + \chi\phi_2(1 - \phi_2)$. The partitioning coefficient is then given by Equation 1.11 with the activity coefficients $\gamma_1 = 1$ and $\gamma_2 = e^{-(2\phi_2\chi/k_B T)}/(1 - \phi_2)$ as well as $K^* = e^{-(\chi - \mu_1^0)/k_B T}$. The relation $\phi_1(\phi)$, together with $\phi_2(\phi) = 2\phi - \phi_1$, is displayed in Figure 1.7 for $K^* = 10$ and three different choices of χ. Note that the tendency of the solute to accumulate in phase '2' is implied by our choice $K^* > 1$. For small ϕ the behavior is ideal and from $\phi_2/\phi_1 = K^*$ and $\phi = (\phi_1 + \phi_2)/2$ we find $\phi_1 = 2\phi/(1 + K^*)$ as well as $\phi_2 = 2\phi K^*/(1 + K^*)$. The ideal behavior is marked in Figure 1.7 by the two dotted lines. For larger ϕ there are deviations from ideal behavior. For $\chi = 0$ (curves *b* and *e* in Figure 1.7) the lattice gas does not exhibit intermolecular interactions. Still, the mole fraction ϕ_2 in the concentrated phase (curve *b*) is smaller than it would be under ideal conditions. The reason is that the

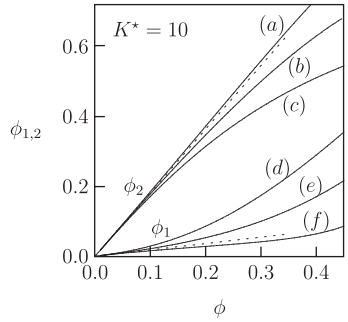

Figure 1.7 *The solute mole fractions $\phi_1(\phi)$ (curves* d–f*) and $\phi_2(\phi)$ (curves* a–c*) of the two phases as function of the total mole fraction $\phi = (\phi_1 + \phi_2)/2$, calculated for $\chi = -1\ k_B T$ (curves* c *and* d*), $\chi = 0$ (curves* b *and* e*), and $\chi = +1\ k_B T$ (curves* a *and* f*). Basis of the calculation is Equation 1.11 with $\gamma_1 = 1$, $\gamma_2 = e^{-(2\phi_2\chi/k_B T)}/(1 - \phi_2)$, and $K^* = 10$. The two dotted lines show the ideal cases, $\phi_1 = 2\phi/(1 + K^*)$ and $\phi_2 = 2\phi K^*/(1 + K^*)$, where the activities are $\gamma_1 = \gamma_2 = 1$.*

non-vanishing solute size implied by the lattice model acts as a hard core repulsion and thus tends to displace solute molecules from the concentrated to the dilute phase. This effective repulsion between solute molecules for $\chi = 0$ is manifested by $\gamma_2 = 1/(1 - \phi_2) > 1$ for $\phi_2 > 0$. For $\chi = -1\ k_BT$ (curves *c* and *d*) the additional repulsive interactions between the solvent molecules further enhance the depletion of solvent molecules from the concentrated phase (curve *c*). In contrast, for $\chi = +1\ k_BT$ (curves *a* and *f*) the solvent molecules attract each other. The attraction overcompensates the hard core repulsion of the solute molecules and thus enriches solute molecules in the concentrated phase (curve *a*) as compared to the ideal case. Indeed, for $\chi = +1\ k_BT$ the activity coefficient $\gamma_2 = e^{-(2\phi_2)}/(1 - \phi_2)$ of the solute in the concentrated phase is below that of an ideal gas ($\gamma_2 = 1$) as long as $\phi_2 \lesssim 0.8$.

1.4.2 Partitioning and Micellization

Consider now the case of drug partitioning into mobile carriers, where the carriers are self-assembled structures such as micelles [38] or polymeric aggregates [37]. We have discussed the cooperative self-assembly of solute molecules in Section 1.3.2. The present section adds the presence of drug molecules that due to their low solubility in water exhibit a tendency to be integrated into the self-assembled aggregates. As in Section 1.3.2, we assume that exactly n solute molecules (we refer to them as surfactants in the following) cooperatively associate into n-mers (i.e., micelles that consist of n surfactants). We now add the presence of drug molecules that are poorly soluble in the solvent but can be integrated into the micelles. There will generally be a maximal number of drug molecules that can be incorporated into a single micelle. To keep the present model transparent, we assume the maximal number to be one. That is, each micelle can carry either one single or no drug molecule. A schematic illustration of the system (monomeric surfactants, monomeric drug molecules, empty micelles, and drug-carrying micelles) is displayed in Figure 1.8. We can express the two processes – micellization in the absence of drug and incorporation of a drug molecule into a micelle – as a system of two chemical reactions

$$n\,\mathrm{A} \overset{K_S}{\rightleftharpoons} \mathrm{A}_n, \quad \mathrm{D} + n\,\mathrm{A} \overset{K_D}{\rightleftharpoons} \mathrm{DA}_n, \tag{1.12}$$

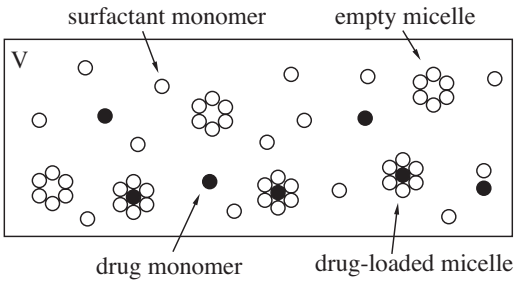

Figure 1.8 *Schematic illustration of surfactants (represented by the symbol ○) and drug molecules (represented by the symbol ●). The surfactants are able to self-assemble into micelles (here displayed with aggregation number n = 6). Each micelle can carry either one or no drug molecule.*

with corresponding equilibrium constants K_S and K_D. We are already familiar from Section 1.3.2 with the reaction on the left-hand side of Equation 1.12. It expresses the association of n monomeric surfactants (each denoted by A) to an empty micelle that consists of n surfactants (denoted by A_n). The reaction on the right-hand side of Equation 1.12 accounts for the assembly of n surfactants and a single drug molecule (denoted by D), resulting in a drug-filled micelle (denoted by DA_n). The mass action law that corresponds to the reaction schemes in Equation 1.12 can be written as

$$\frac{\phi_S^Z}{n(\phi_S^M)^n} = e^{-n(\tilde{\mu}_S^Z - \tilde{\mu}_S^M)/k_BT} = K_S, \quad \frac{\phi_D^Z}{(\phi_D^M)(\phi_S^M)^n} = e^{-(\tilde{\mu}_D^Z - \tilde{\mu}_D^M - n\tilde{\mu}_S^M)/k_BT} = K_D. \quad (1.13)$$

Here, ϕ_S^Z is the mole fraction of surfactant molecules that are engaged in forming empty micelles. (We again use a lattice description as in Section 1.3.2 where each molecule – solvent, surfactant, and drug – occupies one single lattice site). Similarly, ϕ_S^M denotes the mole fraction of monomeric surfactant molecules, ϕ_D^Z denotes the mole fraction of drug molecules that are incorporated into micelles (which equals the mole fraction of the drug-loaded micelles), and ϕ_D^M denotes the mole fraction of monomeric drug molecules. The equilibrium constants K_S and K_D are related to the standard chemical potentials of a surfactant when monomeric ($\tilde{\mu}_S^M$) or incorporated into an empty micelle ($\tilde{\mu}_S^Z$), as well as to the standard chemical potentials per monomeric drug molecule ($\tilde{\mu}_D^M$) and of a drug-filled micelle ($\tilde{\mu}_D^Z$). More specifically, $\triangle g_{empty} = n(\tilde{\mu}_S^Z - \tilde{\mu}_S^M)$ and $\triangle g_{filled} = \tilde{\mu}_D^Z - \tilde{\mu}_D^M - n\tilde{\mu}_S^M$ represent the standard Gibbs free energies of formation for an empty and drug-filled micelle, respectively. The (experimentally fixed) overall mole fractions of surfactants and drug molecules are

$$\phi_S = \phi_S^Z + \phi_S^M + n\phi_D^Z, \quad \phi_D = \phi_D^Z + \phi_D^M, \quad (1.14)$$

respectively. The four relations in Equations 1.13 and 1.14 can be used to calculate the four mole fractions $\phi_S^Z, \phi_S^M, \phi_D^Z, \phi_D^M$. Figure 1.9 shows an example, calculated for $n = 10$, $K_S = 9.76 \times 10^{22}$, $K_D = 10^4 \times K_S$. That implies each surfactant gains a standard Gibbs free energy $\tilde{\mu}_S^M - \tilde{\mu}_S^Z = (k_BT/n) \ln K_S = 5.3\, k_BT$ upon incorporation into an empty micelle. For an entire empty micelle this amounts to $\triangle g_{empty} = -53\, k_BT$. Formation of a drug-loaded micelle gains a standard Gibbs free energy $\triangle g_{filled} = -k_BT \ln K_D = -62\, k_BT$. Hence, incorporating a single drug molecule into an initially empty micelle is associated with an energy gain of $(62 - 53)k_BT = 9k_BT$.

The left diagram of Figure 1.9 displays the mole fractions ϕ_S^M (mole fraction of monomeric surfactants), ϕ_S^Z (mole fraction of surfactants in empty micelles), and $n\phi_D^Z$ (mole fraction of surfactants in drug-loaded micelles) as function of ϕ_s for fixed $\phi_D = 0.2 \times 10^{-3}$. The inset shows the corresponding mole fractions ϕ_D^M (mole fraction of monomeric drug) and ϕ_D^Z (mole fraction of drug in micelles). Clearly, for $n = 10$ there is a well-established CMC (roughly at $\phi_S = 2 \times 10^{-3}$), above which micelle formation starts. Immediately above the CMC there is a region (roughly for $2 \times 10^{-3} < \phi_S < 4 \times 10^{-3}$) where there are slightly more drug-filled than empty micelles. Yet, the majority of drug molecules are still monomeric. At $\phi_S = 4 \times 10^{-3}$ (which is twice the CMC), half of the drug molecules reside in micelles and half of the surfactants are engaged in micelle formation. Of all micelles 50% are drug-loaded. This is the optimal case. Further increasing the overall number of

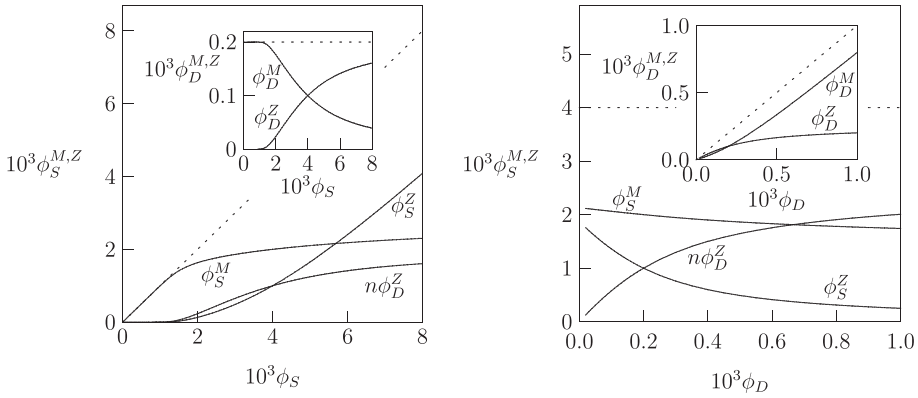

Figure 1.9 Left*: Mole fraction of monomeric surfactants ϕ_S^M, mole fraction of surfactants in empty micelles ϕ_S^Z, and mole fraction of surfactants in drug-loaded micelles $n\phi_D^Z$, displayed as function of the overall mole fraction of surfactants ϕ_S. The inset shows the corresponding mole fraction of monomeric drug ϕ_D^M, and mole fraction of drug in micelles ϕ_D^Z. It is $\phi_D = 0.2 \times 10^{-3}$ in both the main figure and inset.* Right*: Mole fractions ϕ_S^M, ϕ_S^Z, $n\phi_D^Z$, ϕ_D^M, and ϕ_D^Z (the latter two are displayed in the inset) as function of the overall mole fraction of drug molecules ϕ_D, derived for fixed $\phi_S = 4 \times 10^{-3}$. All calculations (in both diagrams) use $n = 10$, $K_S = 9.76 \times 10^{22}$, and $K_D = 10^4 \times K_S$. The dotted lines refer to either ϕ_S or ϕ_D.*

surfactants, ϕ_S, leads to more drug becoming incorporated into micelles but also drastically increases the number of empty micelles.

The right diagram of Figure 1.9 (including the inset) shows the mole fractions ϕ_S^M, ϕ_S^Z, $n\phi_D^Z$, ϕ_D^M, and ϕ_D^Z as function of ϕ_D for fixed $\phi_S = 4 \times 10^{-3}$. As we have discussed above, at $\phi_D = 0.2 \times 10^{-3}$ half of all drug molecules reside in micelles, half of the surfactants form micelles, and half of all micelles contain drug. For $\phi_D < 0.2 \times 10^{-3}$ most micelles are empty and for $\phi_D > 0.2 \times 10^{-3}$ most drug molecules do not reside in micelles. Note also that the total number of micelles is only slightly increased upon increasing ϕ_D. Still, some initially monomeric surfactants become engaged in forming micelles when hydrophobic drug molecules are added to the system.

1.4.3 Hydrophobicity and Ordering of Water

Water solubility is one of the key characteristics in drug design [40]. Yet, what is the physical origin of poor water solubility? Water is a polar molecule that preferentially forms a highly dynamic tetrahedral network of hydrogen bonds between the nonbonding, electron-rich oxygen orbitals and the electron-deficient hydrogen atoms. Hydrogen bonding is sufficiently strong so that in the vicinity of an apolar surface (which is not able to engage in hydrogen bonds) water attempts to maintain or even increase the average number of hydrogen bonds, yet at the cost of being accommodated in a more structured configuration [41, 42]. That is, water rearranges in the vicinity of a hydrophobic solute, forming ordered solvation shells (sometimes also referred to as 'clathrates' or 'cages') that essentially preserve their enthalpy, yet at the cost of a reduced entropy. The interaction of hydrophobic solutes with

their aqueous environment is thus dominated by entropy. As a rough approximation the free energy of transfer of a hydrophobic solute from an oily phase to water (the so-called solvation free energy is proportional to the solute's water-accessible surface area [43]. The corresponding order of magnitude is equal to the surface tension between water and air ($\approx 17 k_B T/\text{nm}^2$). Modeling the underlying physics of solvation has been [44] and continues to be [45, 46] an area of active research. We point out that these first-principle models are very different in nature (and must be distinguished) from descriptor-based models such as ASMS (aqueous solubility based on molecular surface), ASM-SAS (aqueous solubility model based on solvent accessible surface areas), and others, which aim to pre-select drugs prior to high throughput screenings [47].

Can we use simple phenomenological models to describe the solvation of solute molecules? A number of approaches are available. Among them are solvation models that incorporate the dipolar properties of water into continuum electrostatics [48, 49]. Another, (particularly instructive) approach, the so-called Mercedes-Benz model, has been suggested by Dill and coworkers [50]. Yet, here we suffice to briefly mention the most basic phenomenological model which goes back to Marcelja and Radic [51]. It describes water by a vectorial order parameter $\mathbf{P} = \{P_x, P_y, P_z\}$ and – assuming a small perturbation – employs a quadratic form of the free energy

$$F = C \int_V dv \left[\xi^2 (\nabla \cdot \mathbf{P})^2 + \mathbf{P}^2\right]. \tag{1.15}$$

Here, C is a constant and ξ is a characteristic length for the decay of the water perturbation ($\xi \approx 0.2$nm [52]). Minimization of F leads to the vectorial differential equation $\xi^2 \nabla^2 \mathbf{P} = \mathbf{P}$. For example, assume a single planar surface is located at $z = 0$ and imposes an order parameter $\mathbf{P} = \{0, 0, P_0\}$ at the surface ($z = 0$). The order parameter is then $\mathbf{P} = \{0, 0, P_0 e^{-z/\xi}\}$, and the corresponding free energy per unit area (i.e., the surface tension) becomes $C P_0^2 \xi$. Despite being so simple, Marcelja's model correctly predicts the water-mediated repulsion between two identical hydrophilic surfaces as a function of their mutual distance (which has been measured accurately using the surface force apparatus [52]). It also allows for the possibility of attractive water-mediated interactions for hydrophilic surfaces that induce opposite surface orientations of the order parameter. Clearly, the model can serve as a conceptual starting point and reference for more detailed descriptions of water.

1.5 Ways to Model Interactions in Colloidal Systems

In the previous section structural and material properties (partitioning equilibria, CMC, etc) appeared in the form of standard chemical potentials μ_i^0 (see Equation 1.5) and activities γ_i (see Equation 1.11). Their magnitudes result from an often complex interplay of colloidal interactions that include – besides the hydrophobic effect as discussed above – also van der Waals and steric interactions, as well as electrostatic and packing energies of linear chain-like molecules [17, 18]. In the following we focus only on the latter two. That is, we briefly discuss methods to model electrostatic interactions and chain-packing energies and what we can learn from such approaches in terms of designing delivery vehicles for poorly water-soluble drug molecules.

1.5.1 Electrostatic Interactions: The Poisson–Boltzmann Model

Although poorly water-soluble drugs are typically uncharged, electrostatic interactions are essential for the stability of drug carriers, partitioning equilibria, and release mechanisms. According to basic electrostatics, the electric potential $\Phi = \Phi(\mathbf{r})$ can be calculated in a medium of uniform dielectric constant ϵ_W (with $\epsilon_W = 80$ in water) from a given local volume charge density $\rho(\mathbf{r})$ at position $\mathbf{r} = \{x, y, z\}$ using Poisson's law $\nabla^2\Phi = -\rho/(\epsilon_W\epsilon_0)$, where $\nabla^2 = \partial^2/\partial x^2 + \partial^2/\partial y^2 + \partial^2/\partial z^2$ is the Laplacian and $\epsilon_0 = 8.85 \times 10^{-12} As/(Vm)$ is the permittivity of free space. It is convenient to switch from Φ and ϵ_W and to the dimensionless potential $\Psi = e\Phi/k_BT$ and Bjerrum length $l_B = e^2/(4\pi\epsilon_W\epsilon_0 k_BT)$, where e denotes the elementary charge. The Bjerrum length is the distance at which two individual elementary charges have an interaction energy of k_BT. At room temperature $l_B \approx 0.7$ nm in water and $l_B \approx 56$ nm in vacuum. In terms of the dimensionless potential and the Bjerrum length, Poisson's equation reads $\nabla^2\Psi = -4\pi l_B\rho/e$. If the potential Ψ is known we can calculate the energy stored in the corresponding electric field through $U = k_BT \int dv\,(\nabla\Psi)^2/(8\pi l_B)$, where $\nabla = (\partial/\partial x, \partial/\partial y, \partial/\partial z)$ denotes the gradient and where the integration runs over all space.

Aqueous solutions usually contain mobile charges such as counterions or salt. Because of their mobility, the positions of these charge carriers are not known. For example, consider the presence of monovalent cations and anions in a large aqueous volume V, with local concentrations $n_+ = n_+(\mathbf{r})$ and $n_- = n_-(\mathbf{r})$, respectively, and bulk concentration n_0 (both bulk concentrations need to be equal to ensure electroneutrality). The local volume charge density is then $\rho = e(n_+ - n_-)$ (and $\rho = 0$ in the bulk). Hence, to solve Poisson's equation for Ψ we first need to know n_+ and n_-. The mobile ions can, as a first approximation (more accurate is the term *mean-field approximation*), be described as an ideal gas with corresponding entropies $S_+ = -k_B \int_V dv\, n_+[\ln(n_+/n_0) - 1]$ and $S_- = -k_B \int_V dv\, n_-[\ln(n_-/n_0) - 1]$, where the integrations run over the aqueous region V that is accessible to the mobile ions. Because the entropies of an ideal gas mixture are additive, the total entropy is $S = S_+ + S_-$, and the total thermodynamic potential of the system $F = U - TS$ becomes

$$\frac{F}{k_BT} = \int_V dv \left[\frac{(\nabla\Psi)^2}{8\pi l_B} + n_+ \ln\frac{n_+}{n_0} - n_+ + n_- \ln\frac{n_-}{n_0} - n_- + 2n_0 \right]. \qquad (1.16)$$

This expression of the free energy depends on the yet unknown concentrations n_+ and n_- (also Ψ depends on n_+ and n_- through Poisson's equation). In a thermodynamic sense n_+ and n_- constitute two unconstrained degrees of freedom. Hence, in thermal equilibrium F must adopt its minimum with respect to n_+ and n_-. One can show [53] that F becomes minimal for the Boltzmann distributions $n_+ = n_0 e^{-\Psi}$ and $n_- = n_0 e^{\Psi}$. Inserting these into Poisson's equation yields the Poisson–Boltzmann equation

$$l_D^2 \nabla^2 \Psi = \sinh \Psi, \qquad (1.17)$$

where $l_D = (8\pi l_B n_0)^{-1/2}$ is the Debye screening length. Equation 1.17 is a partial differential equation that usually must be solved numerically within the aqueous region; analytical solutions are available only for a few basic geometries [54]. Boundary conditions for Equation 1.17 reflect the presence of macroions in solution. Typical macroions are bodies of low dielectric constant ϵ_L with surface charge density σ at the surface. Because of $\epsilon_W \gg \epsilon_L$ the boundary condition can, approximately, be written $(\partial\Psi/\partial n)_A = -4\pi l_B\sigma/e$, where the

partial derivative of Ψ is taken at the macroion surface A along the surface normal direction, denoted by n and pointing into the aqueous region. Once $\Psi(\mathbf{r})$ is known, the local concentrations n_+ and n_- can be calculated, and the free energy F can be computed according to Equation 1.16. In fact, an equivalent but sometimes more convenient way to compute the free energy is through a so-called *charging process* [18] $F = \int_A do \int_0^\sigma d\bar{\sigma}\, \Phi_0(\bar{\sigma})$, where the equilibrium potential $\Psi_0 = \Psi(x = 0)$ [or, equivalently, $\Phi_0 = \Phi(x = 0)$] needs to be known only at the macroion surface A as function of the surface charge density σ. Increasing σ from zero to its final value and integrating the corresponding surface potential Φ_0 over the macroion surface A then yields the free energy F. A conceptually important limiting case is the Debye-Hückel approximation, which assumes small potential $\Psi \ll 1$ (corresponding to $\Phi \ll 25$ mV) and turns Equation 1.17 into the linear Debye-Hückel equation $l_D^2 \nabla^2 \Psi = \Psi$. In this limit $\Phi_0 \sim \sigma$ and the charging process $\int_0^\sigma d\bar{\sigma}\, \Phi_0(\bar{\sigma}) = \sigma\, \Phi_0(\sigma)/2$ can be carried out. The free energy in the Debye-Hückel limit is thus $F = (1/2) \int_A do\, \sigma\, \Phi_0$, where the integration extends over the macroion surface.

We illustrate the use of the Poisson–Boltzmann model for two examples. The first is a charged lipid layer that we model as a (sufficiently large) single planar surface with charge density σ. For anionic lipids $\sigma < 0$, and for cationic lipids $\sigma > 0$. The lipid layer is in contact with an aqueous region that contains monovalent salt ions of bulk concentration n_0. The potential $\Psi = \Psi(x)$ depends only on the distance x to the surface. It fulfills the Poisson–Boltzmann equation $l_D^2 \Psi''(x) = \sinh \Psi(x)$ with the boundary conditions $\Psi(\infty) = 0$ and $\Psi'(0) = -4\pi l_B \sigma/e$. Here, the second derivative of $\Psi''(x)$ corresponds to the Laplacian (∇^2) in one single dimension, and $\Psi'(0)$ denotes the first derivative of the potential taken at position $x = 0$. A first integration of the Poisson–Boltzmann equation, subject to $\Psi(\infty) = 0$, yields $\Psi'(x) = -(2/l_D) \sinh[\Psi(x)/2]$. At $x = 0$ this equation can be combined with the second boundary condition, implying $\Psi(0) = 2\text{arsinh}(2\pi l_B l_D \sigma/e)$. Yet, this exactly is the surface potential $\Psi_0(\sigma) = \Psi(x = 0, \sigma)$ as a function of the surface charge density that allows us to compute the free energy through the charging process $F = \int_A do \int_0^\sigma d\bar{\sigma}\, \Phi_0(\bar{\sigma}) = k_B T\, A/e \int_0^\sigma d\bar{\sigma}\, \Psi_0(\bar{\sigma})$. Denoting the total lateral area of the lipid layer by A and using the expression of the surface potential, we obtain the free energy per unit area

$$\frac{F}{Ak_BT} = \frac{2}{e} \int_0^\sigma d\bar{\sigma}\ \text{arsinh}\left(2\pi l_B l_D \frac{\bar{\sigma}}{e}\right) = \frac{1}{\pi l_B l_D}\ \left[1 - \sqrt{1+p^2} + p\ \text{arsinh}(p)\right], \quad (1.18)$$

where we have defined the dimensionless quantity $p = 2\pi l_B l_D \sigma/e$. Note that positive and negative surface charge density σ corresponds to positive and negative sign of p, respectively. Although the derivation of F did not require calculation of the potential $\Psi(x)$, we can easily do so by performing a second integration of the Poisson–Boltzmann equation, which yields

$$\Psi(x) = 2 \ln \left\{1 + \frac{2}{e^{x/l_D} \coth\left[\text{arsinh}(p)/2\right] - 1}\right\}. \quad (1.19)$$

We also note the linearized Debye-Hückel results, $\Psi(x) = 2p\, e^{-x/l_D}$ and $F/(Ak_BT) = 2\pi l_B l_D\, (\sigma/e)^2$, which follow from Equations 1.18 and 1.19 in the limit of small p. Here, the potential decays exponentially, and we indeed identify l_D as the corresponding screening length. Note that linearization generally overestimates the magnitude of the potential Ψ.

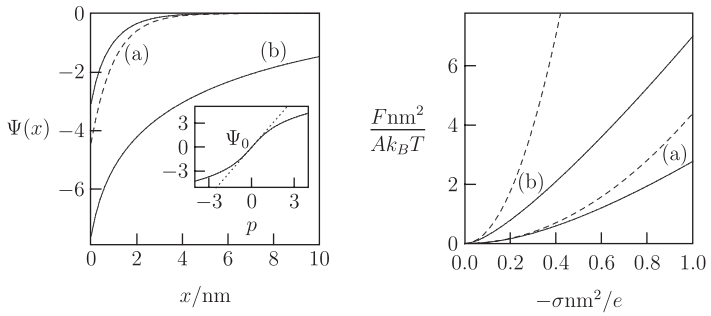

Figure 1.10 *The (dimensionless) potential* $\Psi(x)$ *as function of* x *for* $\sigma = -0.5e/nm^2$ *(left diagram) and the free energy per unit area* $F/(Ak_BT)$ *as function of* $-\sigma/e$ *(right diagram). Both diagrams are calculated for* $l_B = 0.7$ *nm; curves* a *correspond to* $l_D = 1$ *nm, and curves* b *correspond to* $l_D = 10$ *nm. Solid and broken lines correspond to the nonlinear (Poisson–Boltzmann) case and linearized (Debye-Hückel) approximation. (The broken line for case (b) in the left diagram is located outside the displayed region;* $\Psi(0) = -44$*). The inset in the left diagram shows the surface potential* $\Psi_0 = \Psi(x = 0)$ *as function of* $p = 2\pi l_B l_D \sigma/e$ *according to Equation 1.19 (solid line) and in the linearized limit (dotted line) where* $\Psi_0 = 2p$*.*

This can be seen in the inset of Figure 1.10 (left diagram) which shows the surface potential $\Psi_0 = \Psi(x = 0)$ according to Equation 1.19 together with the linearized Debye-Hückel result $\Psi_0 = 2p$. The main diagrams of Figure 1.10 display $\Psi(x)$ from Equation 1.19 and F from Equation 1.18 for two different choices of the Debye screening length, $l_D = 1$ nm and $l_D = 10$ nm. Molarity and Debye screening length are connected through $M = (0.304\,\text{nm}/l_D)^2$, so $l_D = 1$ nm corresponds to physiological conditions, and $l_D = 10$ nm to a 1 mM solution. Surface charge densities of $\sigma \lesssim e/\text{nm}^2$ are typically found for biomacroions such as DNA, lipid membranes, or proteins. Figure 1.10 indicates that the linearized Debye-Hückel limit works reasonably well for $l_D = 1$ nm, but even here there are significant deviations from the prediction of the non-linear model.

Our second example addresses a specific question that is of basic relevance also for the formation of carrier vehicles for drug molecules: What is the energetic cost of incorporating a single charged molecule into a hydrophobic cavity that resides in the aqueous solution? Such a cavity arises, for example, in spherical micelles due to the apolar nature of the surfactant's hydrocarbon chains. For simplicity we model the charged molecule as a sphere of radius R_D with z charges uniformly attached to its surface, implying a charge density $\sigma = ze/(4\pi R_D^2)$. The charged molecule is located at the center of the hydrophobic cavity, which we represent by a sphere of radius R_C. We assume that both the charged molecule and the cavity have the same dielectric constant ϵ_L (with $\epsilon_L \ll \epsilon_W$). We ask the question how much free energy $\triangle F$ it would cost to incorporate the charged molecule into the cavity, starting from a separated state as illustrated in Figure 1.11. To make our final result physically insightful, we shall perform the calculation of $\triangle F$ within the linear Debye-Hückel approximation. We first calculate the free energy of the charged molecule when residing within the cavity; see the right diagram of Figure 1.11. Because of the spherical symmetry the potential depends only on the radial distance r from the center of the charged sphere. The potential $\Psi_o(r)$ outside the cavity ($R_C < r < \infty$) fulfills the Debye-Hückel

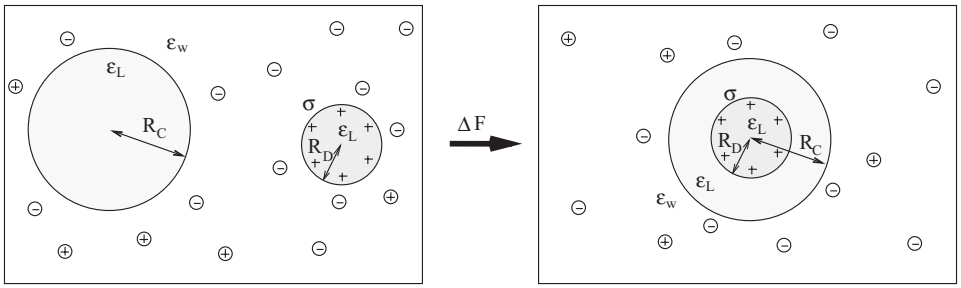

Figure 1.11 *Schematic illustration of a spherical cavity (of radius R_C and dielectric constant ϵ_L) and a charged spherical particle (of radius R_D, dielectric constant ϵ_L, and surface charge density σ). Cavity and particle are initially separated (see the* left diagram*). Inserting the particle into the cavity (see the* right diagram*) incurs a free energy cost $\triangle F$.*

equation $\Psi_o''(r) + (2/r)\Psi_o'(r) = \Psi_o(r)/l_D^2$. Similarly, the potential $\Psi_i(r)$ inside the cavity ($R_D < r < R_C$) fulfills the Laplace equation $\Psi_i''(r) + (2/r)\Psi_i'(r) = 0$. The corresponding boundary conditions are $\Psi_i(R_C) = \Psi_o(R_C)$, $\Psi_o(\infty) = 0$, $\epsilon_W \Psi_o'(R_C) - \epsilon_L \Psi_i'(R_C) = 0$, and $\Psi_i'(R_D) = -l_B z \epsilon_W/(R_D^2 \epsilon_L)$. The latter two account for the change in the dielectric constant at $r = R_C$ and for the presence of the surface charges at $r = R_D$. The solution can be written as

$$\Psi_i(r) = \frac{z l_B}{R_C}\left[\frac{\epsilon_W}{\epsilon_L}\left(\frac{R_C}{r} - 1\right) + \frac{1}{1 + \frac{R_C}{l_D}}\right], \quad \Psi_o(r) = \frac{z}{1 + \frac{R_C}{l_D}} \frac{l_B}{r} e^{\frac{R_C - r}{l_D}}. \quad (1.20)$$

As argued above, the free energy in the Debye-Hückel limit can be calculated according to $F = (1/2)\int_A do\, \sigma \Phi_0$, where the integration runs over the surface $A = 4\pi R_D^2$ of the charged molecule and $\Phi_0 = k_B T \Psi_i(R_D)/e$. Hence,

$$\frac{F}{k_B T} = \frac{z}{2}\Psi_i(R_D) = \frac{z^2 l_B}{2}\left[\frac{\epsilon_W}{\epsilon_L}\left(\frac{1}{R_D} - \frac{1}{R_C}\right) + \frac{1}{R_C\left(1 + \frac{R_C}{l_D}\right)}\right]. \quad (1.21)$$

The first contribution to the free energy in Equation 1.21 is the energy of a spherical capacitor, the second contribution arises due to the diffuse layer of mobile anions in the aqueous solution. In the separated state, see the left diagram of Figure 1.11, potential and thus energy of the cavity vanish, and the energy of the charged particle (which now is immersed in the aqueous solution) can be obtained from Equation 1.21 by replacing $R_C \to R_D$. Hence, we obtain our final result for the change in free energy

$$\frac{\triangle F}{k_B T} = \frac{z^2 l_B}{2}\left[\frac{\epsilon_W}{\epsilon_L}\left(\frac{1}{R_D} - \frac{1}{R_C}\right) + \frac{1}{R_C\left(1 + \frac{R_C}{l_D}\right)} - \frac{1}{R_D\left(1 + \frac{R_D}{l_D}\right)}\right]. \quad (1.22)$$

Note that $\triangle F$ is positive because the energy penalty of the spherical capacitor (the first term in Equation 1.22) overcompensates the energy gain in the diffuse counterion layer. In fact, because of $\epsilon_W \gg \epsilon_L$ the energy cost $\triangle F$ is not only dominated by the capacitor energy but also becomes prohibitively large. For example, $z = 5$, $l_B = 0.7$ nm, $l_D = R_D = 1$ nm,

$R_C = 1.5$ nm, $\epsilon_W = 20\epsilon_L$ yield $\triangle F/k_BT = 58 + 2 - 4 = 56$, or more than $10k_BT$ per charge. Although this model is certainly oversimplified, it correctly captures the high energy cost that is associated with inserting small charged molecules from the aqueous environment intro hydrophobic cavities. Similar arguments also rationalize the permeability barrier that prevents the crossing of lipid bilayers by charged molecules [55].

1.5.2 Chain Packing Model

Carriers for poorly water-soluble drug molecules are often composed of chain-like molecules such as surfactants or polymers. This is the case for micelles, liposomes, and polymeric aggregates. Inserting a drug molecule into such an aggregate perturbs the packing properties of the chains. We briefly discuss the corresponding energy penalty that arises from this perturbation. To this end, we focus on a mean-field model for chain packing in amphiphilic aggregates [56]. The model ignores chain-chain correlations and assumes a uniform density of chain segments everywhere in the aggregate. Both are reasonable assumptions well above the main transition temperature [57]. The starting point of the model is an aggregate of given geometry that is composed of a fixed number N of surfactants with their chains residing in the fluid state. Thus, the hydrocarbon chains are flexible and able to adopt a large number of different conformations. In addition, although the chains are anchored to the aggregate's interface A, the local surface density of surfactant headgroups is able to adjust. Yet, because N is given, the average headgroup density $\bar{\sigma} = N/A$ on the interface A is must be fixed. The most relevant case with regard to modeling a delivery vehicle for drug molecules is the additional presence of rigid bodies (i.e., drug molecules) in the hydrophobic core. The left diagram of Figure 1.12 illustrates such a case, where a long cylinder-like inclusion (of radius R) is immersed into the hydrocarbon core of a lipid bilayer with a certain penetration depth p. What is the perturbation energy of the chain packing when inserting the cylinder-like inclusion into the membrane, and how does that energy depend on the penetration depth?

The central quantity of the mean-field chain packing model is the probability $P(\mathbf{r}, \alpha)$ of a given hydrocarbon chain being anchored at position $\mathbf{r}$ on the polar-apolar interface A and residing in a conformation α. We normalize this probability according to $\int_A d^2\mathbf{r} \sum_\alpha P(\mathbf{r}, \alpha) = A$ where the integration $\int_A d^2\mathbf{r}$ extends over the polar-apolar interface of the aggregate (which is represented by an infinitely thin sheet of surface area A) and the summation runs over all possible chain conformations α. For known $P(\mathbf{r}, \alpha)$ we can calculate the local area density of amphiphiles on the surface according to $\sigma(\mathbf{r}) = \bar{\sigma} \sum_\alpha P(\mathbf{r}, \alpha)$, and the total number of amphiphiles in the aggregate is then $N = \int_A d^2\mathbf{r}\sigma(\mathbf{r}) = \bar{\sigma} A$. The conformational free energy of the N chains can be expressed as the sum of the internal chain energy and an entropic contribution

$$F = U - TS = \frac{N}{A} \int_A d^2\mathbf{r} \sum_\alpha P(\mathbf{r}, \alpha) \left[\epsilon(\alpha) + k_BT \ln P(\mathbf{r}, \alpha)\right]. \tag{1.23}$$

Here, $\epsilon(\alpha)$ denotes the trans-gauge isomerization energy of a chain in conformation α. In thermal equilibrium, F adopts a minimum with respect to the probability distribution $P(\mathbf{r}, \alpha)$. Yet, before the minimization can be carried out, we must account for the additional constraint of constant chain segment density everywhere in the hydrocarbon core (thereby excluding the inserted inclusion). If we denote by $\phi(\alpha, \mathbf{r}', \mathbf{r})$ the number of chain segments

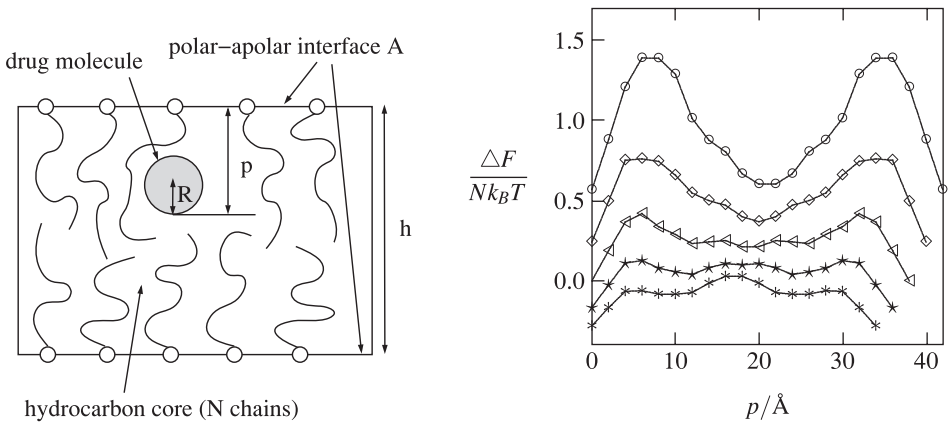

Figure 1.12 Left*: Schematic illustration of a surfactant bilayer with an inserted drug molecule. Shown is a unit cell with N surfactant molecules per drug molecule. The drug molecule is modeled as a long cylinder-like rigid inclusion (shown is the cross-section of the cylinder). The cylinder radius is R, and the hydrocarbon core of the bilayer has thickness h. The penetration depth of the inclusion is p, defined so that for* $p = (h/2) + R$ *the inclusion resides right in the center of the bilayer. Note that the hydrocarbon chains can adopt many different conformations, subject to being packed uniformly on average and remaining within the hydrocarbon core, excluding the rigid cylinder.* Right*: Change in chain conformational free energy* $\triangle F/(Nk_BT)$ *induced by inserting the cylinder-like inclusion into the bilayer, calculated for a system of* $N = 80$ *surfactant chains [of structure* $-(CH_2)_{13} - CH_3$*] per inclusion and plotted as function of the inclusion's penetration depth p. The different curves correspond to* $h = 22$ *Å (*$*$*),* $h = 24$ *Å (*$*$*),* $h = 26$ *Å (*$\triangleleft$*),* $h = 28$ *Å (*$\diamond$*), and* $h = 30$ *Å (*$\circ$*). Reproduced with permission from [58].*

at point $\mathbf{r}'$ within the hydrocarbon core contributed from a surfactant that is located at point $\mathbf{r}$ on the interface A and resides in conformation α, we can compute the average segment density at point $\mathbf{r}'$ through

$$\bar{\phi}(\mathbf{r}') = \int_A d^2\mathbf{r} \sum_\alpha P(\mathbf{r}, \alpha)\phi(\alpha, \mathbf{r}', \mathbf{r}). \tag{1.24}$$

The constraint of constant segment density can then be expressed simply as $\bar{\phi}(\mathbf{r}') = \bar{\phi} = const$ (namely, independent of $\mathbf{r}'$) everywhere in the hydrocarbon chain region, excluding the inserted inclusion. Minimization of F with respect to $P(\mathbf{r}, \alpha)$ and subject to Equation 1.24 yields

$$P(\mathbf{r}, \alpha) = \frac{e^{-\frac{1}{k_BT}\left[\epsilon(\alpha) + \int_V d^3\mathbf{r}\lambda(\mathbf{r})\phi(\alpha, \mathbf{r}', \mathbf{r})\right]}}{\frac{1}{A}\int_A d^2\mathbf{r} \sum_\alpha e^{-\frac{1}{k_BT}\left[\epsilon(\alpha) + \int_V d^3\mathbf{r}\lambda(\mathbf{r})\phi(\alpha, \mathbf{r}', \mathbf{r})\right]}}, \tag{1.25}$$

where the function $\lambda(\mathbf{r})$ is a Lagrangian multiplier that ensures the constraint in Equation 1.24 to be fulfilled. In fact, one finds $\lambda(\mathbf{r})$ by inserting $P(\mathbf{r}, \alpha)$ into Equation 1.24 and

solving the resulting self-consistency relation numerically. This requires the generation of a representative set of chain conformations at various positions along the interface A, based on a molecular model such as Flory's isomeric state model [28]. Once $\lambda(\mathbf{r})$ is known, the probabilities $P(\mathbf{r}, \alpha)$ can be used to compute the free energy according to Equation 1.23. This can be carried out for different choices of the penetration depth ($F(p)$) or in absence of the cylinder (F_{ref}); the difference $\triangle F(p) = F(p) - F_{ref}$ is then the change in chain conformational free energy induced by inserting the cylinder-like inclusion into the bilayer, at given penetration depth p.

The right diagram of Figure 1.12 displays computational results for the change in chain conformational free energy $\triangle F$ of a planar surfactant bilayer as function of the inclusion's penetration depth p. The conformational free energy profile for translation of the inclusion through the bilayer (i.e., changing the penetration depth p) strongly depends on the thickness of the surfactant layer. For a thick layer (see the upper curve in the right diagram of Figure 1.12) the hydrocarbon chains are significantly stretched. The corresponding large entropic penalty can be relieved by placing the inclusion right in the center of the bilayer. Away from that position the free energy exhibits a large barrier. Hence, in bilayers where strong headgroup attractions lead to small cross-sectional area per surfactant, hydrophobic inclusions tend to be located in the center of the bilayer. In contrast, in thin bilayers (see the lower curve in the right diagram of Figure 1.12) the chains from one monolayer dynamically interdigitate into the apposed monolayer. Here, the center exhibits an energy barrier and is thus an unfavorable location. We emphasize that the right diagram of Figure 1.12 displays the energy per surfactant chain. Because the calculation is based on $N = 80$ chains per inclusion, an energy change of, say, $0.2\, k_B T$ would translate into $40\, k_B T$ per inclusion. Hence, the conformational properties of the chains are expected to provide a significant contribution to defining the position of a hydrophobic inclusion within a surfactant aggregate. These considerations apply to liposomes and similarly to micellar aggregates.

1.6 Kinetics of Drug Transfer from Mobile Nanocarriers

The theoretical concepts we have discussed so far refer exclusively to thermodynamic equilibrium. Yet, the delivery of drugs inevitably involves dynamic properties as well. Dynamic properties determine the kinetics, i.e., the retention properties of the delivery vehicle and the amount of drug molecules transferred from the delivery vehicle to a target system as function of time [59]. Modeling the corresponding transfer properties is often accomplished using methods based on chemical reaction kinetics [60].

In the following we consider a simple and instructive scenario, mobile delivery vehicles and mobile targets that are enclosed in a fixed volume V. We will refer to the delivery vehicles as *donors* and to the target system as *acceptors*. We assume that the numbers of both donors (N_D) and acceptors (N_A) remain unchanged. Hence $N_D + N_A = N$ is a fixed constant. Initially, the donors contain a certain number of drug molecules M (or, equivalently, N_D/M drug molecules per delivery vehicle on average), whereas the acceptors are empty. Over time, some of the drug molecules will migrate from the donors to the acceptors. We can describe the corresponding time dependence by the numbers $M_D = M_D(t)$ and $M_A = M_A(t)$ of drug molecules residing in the donors and acceptors,

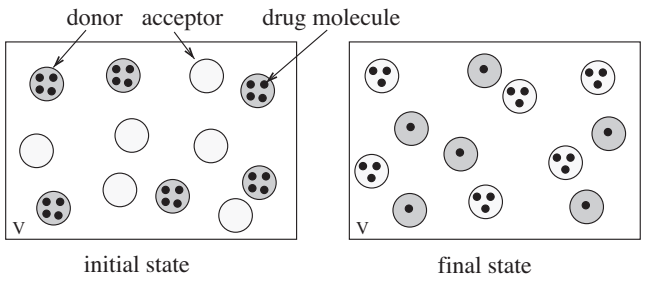

Figure 1.13 *Schematic illustration of drug transfer from N_d donors (dark shaded) to N_a acceptors (light shaded). Drug molecules can reside in either donors or acceptors; they are represented by the dark bullets. Initially (left diagram), all M drug molecules are located inside the donors. The kinetics of drug transfer can be described by the numbers $M_d(t)$ and $M_a(t)$, of drug molecules in donors and acceptors, respectively. After thermal equilibrium is established (right diagram), the drug molecules are distributed between donors and acceptors with an equilibrium distribution $M_d(t \to \infty) = M_d^{eq}$ and $M_a(t \to \infty) = M_a^{eq}$. The displayed example corresponds to $N_d = N_a = 6$ and $M = M_d^{eq} + M_a^{eq} = 6 + 18 = 24$.*

respectively. For poorly water-soluble drugs $M_D(t) + M_A(t) = M$ is a constant, implying that very little drug is dissolved in the aqueous phase. In addition, if the transfer of drug molecules is slow compared to typical diffusion times of donors and acceptors, we may ignore spatial variations of donor and acceptor concentrations. Figure 1.13 shows an illustration of the system. Note that we make a number of significant assumptions (including the fixed volume, the presence of only one type of mobile target system, the slow transfer dynamics of the drugs between donors and acceptors, and the fixed numbers of donors and acceptors). Yet, our system still provides a convenient starting point as it is a generic model for various types of mobile drug delivery vehicles such as liposomes, micelles, and polymeric aggregates.

It is generally useful to distinguish between the dynamics of drug transport within a single delivery vehicle (such as the flip-flop of drug molecules between the two leaflets of a liposomal membrane) and the dynamics of transport from the delivery vehicle to a target site. The latter involves two principal mechanism, namely transfer through collisions and transfer through diffusion [61]. Both are illustrated in Figure 1.14. Note that the collision mechanism requires temporary physical contact between a donor and acceptor (or, similarly,

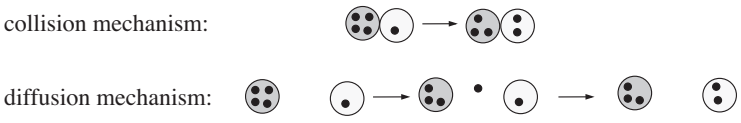

Figure 1.14 *Schematic illustration of the collision and diffusion mechanisms for the transfer of drugs from donor (*dark shaded*) to acceptor (*light shaded*). Drug molecules are represented by filled bullets. The collision mechanism involves direct drug transfer upon the collision of donor and acceptor. For the diffusion mechanism, drug molecules are first released into the aqueous phase. In a second step they are taken up by the acceptor.*

donor-donor or acceptor-acceptor), whereas the diffusion mechanism involves drug molecules transferring via the intermediate step of diffusing through the aqueous environment. Both mechanisms have been invoked to explain the transport of lipids and cholesterol [62] between membranes. Let us discuss a model for the kinetics of the collision and diffusion mechanisms.

1.6.1 Collision Mechanism

Because of the need for individual collision between pairs of donor-donor, donor-acceptor or acceptor-acceptor, the kinetics of the collision mechanism is based on a second-order process. Specifically, if only d_i donors that each contain i drug molecules and a_j acceptors that each contain j drug molecules are present, the collision rate between donors and acceptors is proportional to the product $d_i a_j$. If donors and acceptors of given distributions d_i and a_j are present, then all possible combinations of i and j will contribute to the collision rate. Any modeling effort requires knowledge of how the proportionality factor depends on i and j. Typically, it simply reflects the concentration difference. This ignores any nonideal behavior (such as aggregation of the drug molecules in the donors or acceptors), but it allows us to express the resulting kinetic equations only in terms of $M_d(t)$ and $M_a(t)$. The result [63]

$$\frac{dM_d}{dt} = \frac{K_{coll}}{V}(M_a N_d - M_d N_a + k N_a N_d), \quad \frac{dM_a}{dt} = \frac{K_{coll}}{V}(M_d N_a - M_a N_d - k N_a N_d), \tag{1.26}$$

contains two constants: a unit transfer rate K_{coll} and the difference k of drug molecules carried on average by each donor and acceptor in thermal equilibrium (i.e., $k = 2$ in the schematic representation of Figure 1.13). The solution of Equations 1.26

$$M_a(t) = M - M_d(t) = \left(1 - e^{-\frac{N}{V} K_{coll}\, t}\right) \frac{N_a}{N}\,(M - k N_d). \tag{1.27}$$

corresponds to simple exponential behavior. The equilibrium distributions $M_d^{eq} = M_d(t \to \infty)$ and $M_a^{eq} = M_a(t \to \infty)$ indeed fulfill the relation $(M_d^{eq}/N_d) - (M_a^{eq}/N_a) = k$, thus verifying our interpretation of k above. We point out that the rate constant $K = K_{coll} N/V$ of the transfer through collisions depends on the total concentration $N/V = (N_d + N_a)/V$ of donors and acceptors. Hence, larger concentrations N/V increase the transfer speed as collisions become more likely.

Equations 1.26 represent a first-order process. The reason for the microscopic second-order collision mechanism to translate into a first-order process for the overall kinetic behavior is the conservation of the numbers N_D and N_A. That is, collisions do not affect the numbers of 'reactants', namely the donors and acceptors. We can describe the transfer of drug molecules from donors (D) to acceptors (A) by the chemical reaction scheme

$$\mathrm{D} \underset{K_2}{\overset{K_1}{\rightleftharpoons}} \mathrm{A} \tag{1.28}$$

with rate constants $K_1 = (1 - k N_d/M)\, K N_a/N$ and $K_2 = (1 + k N_a/M)\, K N_d/N$. The corresponding equilibrium constant $K_{eq} = K_1/K_2 = (M - k N_d)/(M + k N_a)$ allows us to calculate the standard Gibbs free energy $\triangle g^0 = k_B T \ln[(M/N_d + k)/(M/N_a - k)]$. Specifically, if donors and acceptors are chemically similar, $k = 0$ and $\triangle g^0 = k_B T \ln(N_d/N_a)$

contains only an entropic component. For $N_d > N_a$ we have $\triangle g^0 > 0$. More drugs will reside in the donors simply because more donors are available. An enthalpic component may arise in $\triangle g^0$ through the temperature dependence of k.

1.6.2 Diffusion Mechanism

For the diffusion mechanism the drug molecules pass through the aqueous phase as illustrated in Figure 1.14. If the rates of drug release/uptake of each individual donor and acceptor are strictly proportional to the number of occupied/free binding sites, then the kinetics of the diffusion mechanism can be described according to the chemical reaction scheme

$$\mathrm{D} \underset{K_d^{upt}}{\overset{K_d^{rel}}{\rightleftharpoons}} \mathrm{W} \underset{K_a^{rel}}{\overset{K_a^{upt}}{\rightleftharpoons}} \mathrm{A} \tag{1.29}$$

where the additional water-dissolved state of the drug molecules is denoted by W. Because the drug molecules are poorly water-soluble, it is appropriate to introduce a steady-state approximation $dM_w/dt = 0$, where $M_w(t) \ll M \approx M_a(t) + M_d(t)$ is the number of drug molecules in the aqueous phase. If we also assume equal uptake rates $K_d^{upt} = K_a^{upt}$ of donors and acceptors, we can express the kinetic equations for the diffusion mechanism as

$$\frac{dM_d}{dt} = K_{diff}(M_a N_d - M_d N_a + k N_a N_d), \quad \frac{dM_a}{dt} = K_{diff}(M_d N_a - M_a N_d - k N_a N_d), \tag{1.30}$$

where we have defined $K_d^{rel} = K_{diff}(1 - kN_d/M)$ and $K_a^{rel} = K_{diff}(1 + kN_a/M)$. Comparison with Equations 1.26 reveals that the diffusion mechanism follows the same first-order kinetics as the collision mechanism, yet with a different rate constant K_{diff}. The total rate constant of the combined collision and diffusion process is thus $K = K_{coll}(N/V) + K_{diff}$. The total rate constant K is a measurable quantity; its dependence on the total concentration of donors and acceptors gives insights into the mechanism of drug transfer. A specific example is the transfer of the drug molecule temoporfin (a second generation photosensitizer) from donor liposomes to acceptor liposomes. Transfer experiment have been conducted [64] using radioactive-labeled temoporfin residing initially in donor liposomes. Addition of acceptor liposomes initiates a transfer process that can be measured as a function of time. To this end, donor and acceptor liposomes carry different amounts of charged lipids and can thus be separated from each other using an ion exchange column. The experimental results for $M_a(t)$ can indeed typically be described by a simple exponential function with inverse rate constants K^{-1} on the order of several hours. Analysis of the concentration dependence $K = K(N/V)$ of the rate constant suggested for unilamellar liposomes (consisting mostly of phospholipids and having a diameter of about 100 nm) that for concentrations of $N/V < 200/\mu\mathrm{m}^3$ the transfer was dominated by the diffusion mechanism whereas for $N/V > 200/\mu\mathrm{m}^3$ the collision mechanism was more prevalent [64].

1.6.3 Internal Kinetics

So far, we have assumed that drug molecules in donors and acceptors can reside in only one single state. This may be appropriate for some cases such as lipid bilayers with all

drug molecules buried within the hydrocarbon core; see the upper curve in Figure 1.12. In general, however, there will be a set of either discrete or continuously distributed states in which the drug molecules can reside. The most simple example is a two-state system. Consider, for example, drug molecules that preferentially interact with either the inner or outer leaflet of a liposome; see the lower curve in Figure 1.12. Here, drug molecules initially associated with the inner monolayer need to first flip to the outer monolayer before they can transfer to the target site. Hence a characteristic flip-flop time will enter into the description of the kinetic behavior. A more complex example for the internal dynamics are reservoir systems such as polymeric aggregates [65], hydrogels [66], or microemulsions [67]. Here, the set of accessible states is continuous, and solutions of the diffusion equation determine the availability of the drug molecules at the interface of the carrier with the ambient environment. Different relevant scenarios and theoretical models for these cases have been reviewed recently [23].

Let is briefly discuss the extension of our one-state model for the collision and diffusion kinetics to a two-state model. To make our analysis most instructive, we assume that donors and acceptors are sufficiently large (so that curvature effects can be ignored) and chemically identical liposomes that can host drug molecules in either the inner or outer monolayer; see the illustration on the left-hand side of Figure 1.15. The chemical rection scheme for the transfer of drug molecules from the inner (D^I) to first the outer (D^O) leaflet of the donor liposomes, next to the outer (A^O) to finally to the inner (A^O) leaflets of the acceptor liposomes, can be written as

$$D^I \underset{G}{\overset{G}{\rightleftharpoons}} D^O \underset{K_2}{\overset{K_1}{\rightleftharpoons}} A^O \underset{G}{\overset{G}{\rightleftharpoons}} A^I. \tag{1.31}$$

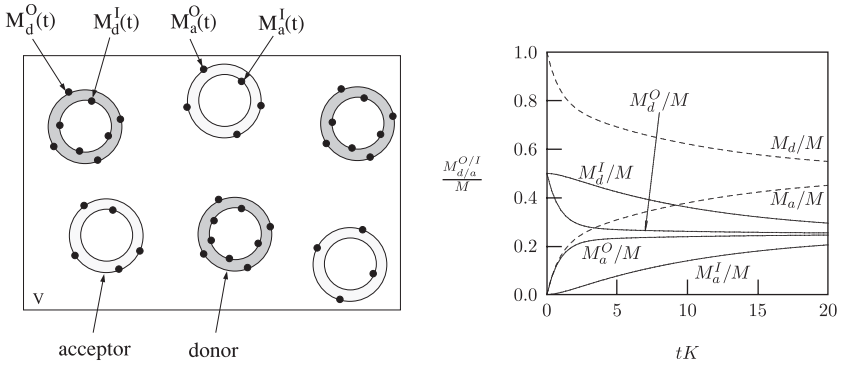

Figure 1.15 Left*: Mixture of N_d donor and N_a acceptor liposomes where the M drug molecules are incorporated either in the inner or outer monolayer. The instantaneous numbers of drug molecules in the inner and outer leaflets of the donor liposomes is denoted by $M_d^I(t)$ and $M_d^O(t)$, respectively. For the acceptor liposomes the corresponding notation is $M_a^I(t)$ and $M_a^O(t)$.* Right*: Plots of $M_d^O(t)$, $M_d^I(t)$, $M_a^O(t)$, and $M_a^I(t)$ according to Eqs. 1.33 for $G/K = 1/10$ and $N_a/N = N_d/N = 0.5$. The broken lines show the biexponential behaviors of the sums $M_d = M_d^O + M_d^I$ and $M_a = M_a^O + M_a^I$. The time is plotted in units of the inverse rate constant K. Note also $\omega_1 = 1.11K$ and $\omega_2 = 0.09K$ are the effective rate constants for the decay. The right diagram is reproduced from [63].*

Here, due to the symmetry of liposomes with regard to the inner and outer leaflet, a single rate constant G fully describes the internal kinetics of the donor and acceptor liposomes. The rate constants for the inter-liposomal transfer are given, as in Equation 1.28 but with $k = 0$ and $K = K_{coll}(N/V) + K_{diff}$, by $K_1 = KN_a/N$ and $K_2 = KN_d/N$. Denote the numbers of drug molecules residing in the inner and outer monolayers of the donor liposomes by $M_d^I(t)$ and $M_d^O(t)$, respectively. For the acceptor liposomes, the corresponding quantities are $M_a^I(t)$ and $M_a^O(t)$. They fulfill the equations

$$\frac{dM_d^O}{dt} = \frac{K}{N}(M_a^O N_d - M_d^O N_a) - G(M_d^O - M_d^I), \quad \frac{dM_d^I}{dt} = G(M_d^O - M_d^I),$$
$$\frac{dM_a^O}{dt} = \frac{K}{N}(M_d^O N_a - M_a^O N_d) - G(M_a^O - M_a^I), \quad \frac{dM_a^I}{dt} = G(M_a^O - M_a^I), \qquad (1.32)$$

which depend only on the two rate constants K and G. Initially, all drug molecules are distributed in the donor liposomes, with 50% in each monolayer. The solution of Equations 1.32 is then

$$M_d^I(t) = \frac{M}{2}\left[\frac{N_d}{N} + \frac{N_a}{N}\,\frac{\omega_2 e^{-\omega_1 t} - \omega_1 e^{-\omega_2 t}}{\omega_2 - \omega_1}\right],$$
$$M_d^O(t) - M_d^I(t) = \frac{M}{2}\,K\,\frac{N_a}{N}\,\frac{e^{-\omega_2 t} - e^{-\omega_1 t}}{\omega_2 - \omega_1},$$
$$M_a^I(t) = \frac{MN_a}{2N}\left[1 - \frac{\omega_2 e^{-\omega_1 t} - \omega_1 e^{-\omega_2 t}}{\omega_2 - \omega_1}\right],$$
$$M_a^O(t) - M_a^I(t) = \frac{M}{2}\,K\,\frac{N_a}{N}\,\frac{e^{-\omega_1 t} - e^{-\omega_2 t}}{\omega_2 - \omega_1}, \qquad (1.33)$$

which describes a biexponential decay with the two effective rate constants ω_1 and ω_2. They follow from G and K through $2G + K = \omega_1 + \omega_2$ and $4G^2 + K^2 = (\omega_2 - \omega_1)^2$. A plot of $M_d^O(t)$, $M_d^I(t)$, $M_a^O(t)$, and $M_a^I(t)$, derived for $G/K = 1/10$ and $N_a/N = N_d/N = 0.5$, is shown in the right diagram of Figure 1.15. In this example, the flip-flop of drug molecules between the liposome leaflets is the rate-limiting step. Hence, the drug molecules in the outer monolayers of donor and acceptor liposomes are quickly exchanged, but it takes much longer to also transfer the drug molecules that initially resided in the inner monolayers of the donor liposomes. It is also interesting to mention two limiting cases. First, for $G = 0$ the drug molecules in the inner leaf do not participate in the transfer, and Equation 1.33 yield $M_d^I(t) = M/2$, $M_a^I(t) = 0$, $M_a^O(t) = M/2 - M_d^O(t) = (1 - e^{-Kt})\,(MN_a)/(2N)$, which corresponds to simple exponential decay for $M/2$ drug molecules. Second, for $G \to \infty$ the drug molecules exchange (i.e., flip-flop) fast between the liposome leaflets. Equations 1.33 then read $M_a^I(t) = M_a^O(t) = M/2 - M_d^I(t) = M/2 - M_d^O(t) = (1 - e^{-Kt/2})\,(MN_a)/(2N)$. Here again, we find simple exponential behavior, yet with an apparent rate constant $K/2$ because only the drug molecules in the outer leaflets contribute to the concentration gradients that drive the transport.

We point out that the present two-state model with the identical donor and acceptor liposomes is perhaps the simplest case that leads to biexponential behavior. Different rate constants G_{donor} and $G_{acceptor}$ or the presence of more internal states can be included in a straightforward matter. Also, the two states introduced in our model may not necessarily correspond to the two leaflets of a lipid membrane. They can refer to any states in which

the drug is able to reside. For example, for temoporfin in PEGylated liposomes Reshetov *et al*. [68] have suggested that only a fraction of the drug molecules reside inside the lipid bilayer whereas the remaining fraction partitions into the PEG shell. This then leads to a fast and slow component in the transfer process. More generally, biexponential behavior is often observed for the release of drug molecules from nanocarriers; for an account of some experimental systems, see Zeng *et al*. [69].

1.7 Conclusion

We reiterate the scope of our present modeling approach: elucidating basic physical principles that are important for the design of drug delivery vehicles. What contribution can this have to the actual design of specific delivery systems, say, the retention of temoporfin in lipid vesicles?

We first point out that the comprehensive modeling of drug delivery (including that of temoporfin) from basic physical principles is currently an illusion. However, there is an ever increasing body of experimental data that calls for understanding and interpretation rather than mere accumulation and classification. The quest for understanding suggests ultimately envisioning a complete physico-chemical modeling framework of self-associating drug carrier systems, including their interactions with the target system. What would need to be included in this model is the specificity of each drug and drug carrier system, including a molecular-level description of the drug's state inside the carrier and the abundance of potential drug acceptor systems, i.e., in the blood after injecting the carrier. This kind of quantitative modeling would inevitably require large-scale computer simulations, where the complex interactions between carriers, carrier formation, drug encapsulation, and interactions with the target system emerge 'naturally' (i.e., as a result of the simulation). Yet even if an incredibly fast computer were, in principle, able to carry out atomistic simulations of an entire organism, the understanding of the underlying principles will still benefit from the simple kind of models that we have discussed in the present chapter.

Second, some of the models described in the present chapter actually can be applied to specific systems, given that experimental data are present to an extent that allows validation of the model approach. Optimally, modeling and experimental verification proceed in parallel, not independently from each other. For example, the identification of the diffusion and collision mechanism for the transfer of temoporfin from donor to acceptor liposomes (see Section 1.6) requires the measurement of rate constants as a function of the *total* concentration of acceptors and donors (instead of only the concentration of acceptor liposomes). Someone who is testing this theory needs to have this information *prior* to carrying out the kinetic transfer experiments. Conversely, modeling of the transfer process is futile unless guided by a set of well-defined experimental conditions (such as the information that liposome fusion normally can be ignored during a kinetic transfer experiment, that the transfer is typically a first-order process, etc.). In addition, the transfer of measurements have to be done in a system undisturbed by the measurement method. Methods which have been described to investigate the *in vitro* drug release of colloidal drug delivery systems, including sample-and-separate methods, membrane-barrier methods, continuous-flow methods and *in situ* methods [70], are for the majority of the methods not adequate as filtration steps

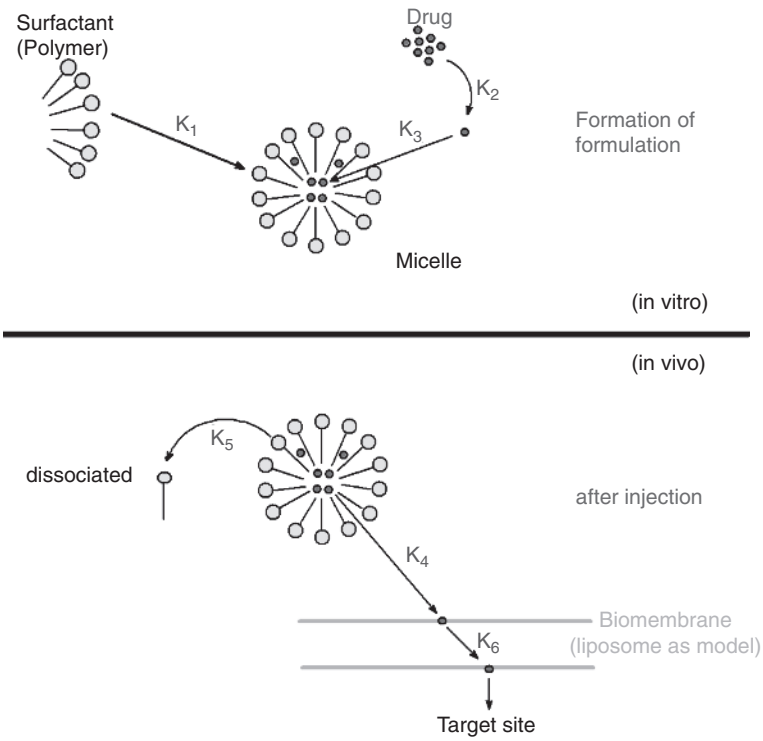

Figure 1.16 Upper part: *Illustration of the* in vitro *formation of a carrier system from surfactants and drug molecules. The drug molecules partition into the micelles or, alternatively, form an aggregate on their own. Different rate constants k_1, k_2 and k_3 are involved in the kinetics of this process*. Lower part: *Illustration of the* in vivo *transfer of drug molecules from a drug-loaded carrier to a biomembrane target. Again, different rate constants k_4, k_5 and k_6 are involved in the kinetics of this process*. (See colour plate section.)

or dialysis membrane barriers introduce a distortion of the real parameters necessary for the modeling process (the described methods are of course usable when comparing and ranking carrier systems). In this respect, fluorescence-based methods (i.e., employing the intrinsic fluorescence of a drug or of the carrier system) offer valuable advantages over invasive methods [19].

The models presented in this chapter may be extended. Recall, for example, the addition of the internal kinetics to the overall transfer kinetics of drugs between mobile nanocarriers (in Section 1.6.3). The final result, see Equations 1.33, depends on the two intrinsic rate constants K and G, corresponding to the transfer between carriers and within each carrier. Already here the final result is of considerable complexity. Yet, many interesting phenomena involve more than two rate constants (and thus even more complexity than Equations 1.33). Figure 1.16 shows two examples, one *in vitro* and one *in vivo*. The first example illustrates the kinetics of forming a carrier system, where surfactants form a micelle and the drug molecules may partition into that micelle or stay in the aqueous phase as monomers or as an aggregate. In contrast to Section 1.4.2, the drug can either partition into the micelle or

form an aggregate on its own. Hence, there is a competition to see which one to include in a theoretical model is more relevant and more interesting than our treatment in Section 1.4.2. It is also more complex, but the present chapter has discussed all the tools needed to write down and analyze the kinetic equations. Similarly for the second example, the interaction of a drug-loaded carrier with a biomembrane target, the kinetic equations do not only involve more than two rate constants, but they also require an understanding of the driving forces of the drug molecules to partition between the carrier and the biomembrane. Again, in the present chapter we have introduced some of the basic concepts that contribute to the modeling of these complex systems.

Acknowledgments

We would like to thank Stephan Loew and Alexander Wagner for insightful discussions.

References

1. C. A. Lipinski. Drug-like properties and the causes of poor solubility and poor permeability. *J Pharmacological Toxicological Methods*, **44**(1), 235–249 (2000).
2. M. J. Lawrence, G. D. Rees. Microemulsion-based media as novel drug delivery systems. *Adv Drug Delivery Rev*, **45**(1), 89–121 (2000).
3. C. X. He, Z. G. He, J. Q. Gao. Microemulsions as drug delivery systems to improve the solubility and the bioavailability of poorly water-soluble drugs. *Expert Opinion On Drug Delivery*, **7**(4), 445–460 (2010).
4. B. Jeong, S. W. Kim, Y. H. Bae. Thermosensitive sol-gel reversible hydrogels. *Adv Drug Delivery Rev*, **54**(1), 37–51 (2002).
5. M. C. Jones, J. C. Leroux. Polymeric micelles: a new generation of colloidal drug carriers. *European J Pharmaceutics Biopharmaceutics*, **48**(2), 101–111 (1999).
6. V. P. Torchilin. Micellar nanocarriers: Pharmaceutical perspectives. *Pharmaceutical Research*, **24**(1), 1–16 (2007).
7. J. A. Zasadzinski, B. Wong, N. Forbes, G. Braun, G. H. Wu. Novel methods of enhanced retention in and rapid, targeted release from liposomes. *Current Opinion in Colloid & Interface Science*, **16**(3), 203–214 (2011).
8. D. E. Discher, V. Ortiz, G. Srinivas, M. L. Klein, Y. Kim, C. A. David, S. S. Cai, P. Photos, F. Ahmed. Emerging applications of polymersomes in delivery: From molecular dynamics to shrinkage of tumors. *Progress in Polymer Science*, **32**(8–9), 838–857 (2007).
9. U. Gupta, H. B. Agashe, A. Asthana, N. K. Jain. Dendrimers: Novel polymeric nanoarchitectures for solubility enhancement. *Biomacromolecules*, **7**(3), 649–658 (2006).
10. R. H. Muller, C. M. Keck. Challenges and solutions for the delivery of biotech drugs: a review of drug nanocrystal technology and lipid nanoparticles. *J Biotechnology*, **113**(1–3), 151–170 (2004).
11. H. Bunjes. Lipid nanoparticles for the delivery of poorly water-soluble drugs. *J Pharmacy Pharmacology*, **62**(11), 1637–1645 (2010).
12. G. Poste, D. Papahadjopoulos. Lipid vesicles as carriers for introducing materials into cultured-cells: Influence of vesicle lipid-composition on mechanism(s) of vesicle

incorporation into cells. *Proc National Acad Sciences United States Am*, **73**(5), 1603–1607 (1976).
13. M. L. Immordino, F. Dosio, L. Cattel. Stealth liposomes: review of the basic science, rationale, and clinical applications, existing and potential. *Int J Nanomedicine*, **1**(3), 297–315 (2006).
14. P. Sapra, T. M. Allen. Ligand-targeted liposomal anticancer drugs. *Progress in Lipid Research*, **42**(5), 439–462 (2003).
15. S. Ganta, H. Devalapally, A. Shahiwala, M. Amiji. A review of stimuli-responsive nanocarriers for drug and gene delivery. *J Controlled Release*, **126**(3), 187–204 (2008).
16. R. R. Sawant, V. P. Torchilin. Liposomes as 'smart' pharmaceutical nanocarriers. *Soft Matter*, **6**(17), 4026–4044 (2010).
17. J. N. Israelachvili. *Intermolecular and Surface Forces.* Second edition. New York: Academic Press (1992).
18. D. F. Evans, H. Wennerstrom. *The Colloidal Domain, Where Physics, Chemistry, and Biology Meet.* Second edition. VCH publishers (1994).
19. S. Petersen, A. Fahr, H. Bunjes. Flow cytometry as a new approach to investigate drug transfer between lipid particles. *Mol Pharmaceutics*, **7**(2), 350–363 (2010).
20. P. van Hoogevest, X. Liu, A. Fahr, M. L. S. Leigh. Role of phospholipids in the oral and parenteral delivery of poorly water soluble drugs. *J Drug Delivery Science Technology*, **21**(1), 5–16 (2011).
21. M. Grassi, G. Grassi, R. Lapasin, I. Colombo. *Understanding Drug Release and Absorption Mechanisms: a Physical and Mathematical Approach.* Boca Raton, FL: CRC Press (2006).
22. Martin Malmsten. *Surfactants and Polymers in Drug Delivery*, volume 122 of *Drugs and the Pharmaceutical Sciences.* New York: Marcel Dekker (2002).
23. J. Siepmann, F. Siepmann. Mathematical modeling of drug delivery. *Int J Pharmaceutics*, **364**(2), 328–343 (2008).
24. G. Bonacucina, M. Cespi, M. Misici-Falzi, G. F. Palmieri. Colloidal soft matter as drug delivery system. *J Pharmaceutical Sciences*, **98**(1), 1–42 (2009).
25. P. A. Kralchevsky, K. D. Danov, N. D. Denkov. Chemical physics of colloid systems and interfaces. In K. S. Birdi, (Ed.) *Handbook of Surface and Colloid Chemistry*, 2 edition, chapter 5. Boca Raton, FL: CRS Press, 137–344 (2003).
26. H. T. Davis. *Statistical Mechanics of Phases, Interfaces, and Thin Films.* New York: VCH publishers (1996).
27. R. DeHoff. *Thermodynamics in Materials Science.* Second edition. Boca Raton, FL: CRC Press (2006).
28. P. J. Flory. *Statistical Mechanics of Chain Molecules.* New York: Wiley-Interscience (1969).
29. D. X. Lin, Y. B. Huang. A thermal analysis method to predict the complete phase diagram of drug-polymer solid dispersions. *Int J Pharmaceutics*, **399**(1–2), 109–115 (2010).
30. S. Patel, A. Lavasanifar, P. Choi. Application of molecular dynamics simulation to predict the compatability between water-insoluble drugs and self-associating poly(ethylene oxide)-b-poly(epsilon-caprolactone) block copolymers. *Biomacromolecules*, **9**(11), 3014–3023 (2008).

31. M. C. Branco, J. P. Schneider. Self-assembling materials for therapeutic delivery. *Acta Biomaterialia*, **5**(3), 817–831 (2009).
32. A. Mahmud, X. B. Xiong, H. M. Aliabadi, A. Lavasanifar. Polymeric micelles for drug targeting. *J Drug Targeting*, **15**(9), 553–584 (2007).
33. R. W. Redmond, E. J. Land, T. G. Truscott. Aggregation effects on the photophysical properties of porphyrins in relation to mechanisms involved in photodynamic therapy. *Adv in Experimental Medicine Biol*, **193**, 293–302 (1985).
34. S. Sasnouski, V. Zorin, I. Khludeyev, M. A. D'Hallewin, F. Guillemin, L. Bezdetnaya. Investigation of Foscan (R) interactions with plasma proteins. *Biochimica Et Biophysica Acta-General Subjects*, **1725**(3), 394–402 (2005).
35. J. N. Israelachvili, D. J. Mitchell, B. W. Ninham. Theory of self-assembly of hydrocarbon amphiphiles into micelles and bilayers. *J Chem Society, Faraday Transactions Ii*, **72**, 1525–1568 (1976).
36. A. Ben-Shaul, W. M. Gelbart. Statistical thermodynamics of amphiphile self-assembly: Structure and phase transitions in micellar solutions. In W. M. Gelbart, A. Ben-Shaul, D. Roux, (Eds.) *Micelles, Membranes, Microemulsions, and Monolayers*, first edition, section 1. New York: Springer, 359–402 (1994).
37. K. A. Dill, S. Bromberg. *Molecular Driving Forces: Statistical Thermodynamics in Chemistry & Biology.* First edition. New York: Garland Publishing (2003).
38. A. Muellertz, A. Ogbonna, S. Ren, T. Rades. New perspectives on lipid and surfactant based drug delivery systems for oral delivery of poorly soluble drugs. *J Pharmacy Pharmacology*, **62**(11), 1622–1636 (2010).
39. K. Kataoka, A. Harada, Y. Nagasaki. Block copolymer micelles for drug delivery: design, characterization and biological significance. *Adv Drug Delivery Rev*, **47**(1), 113–131 (2001).
40. S. N. Bhattachar, L.A. Deschenes, J. A. Wesley. Solubility: it's not just for physical chemists. *Drug Discovery Today*, **11**(21–22), 1012–1018 (2006).
41. P. R. Bergethon. *The Physical Basis of Biochemistry: The Foundations of Molecular Biophysics.* First edition. New York: Springer Verlag (1998).
42. D. Chandler. Interfaces and the driving force of hydrophobic assembly. *Nature*, **437**(7059), 640–647 (2005).
43. K. A. Sharp, A. Nicholls, R. F. Fine, B. Honig. Reconciling the magnitude of the microscopic and macroscopic hydrophobic effects. *Science*, **252**(5002), 106–109 (1991).
44. D. Sitkoff, K. A. Sharp, B. Honig. Accurate calculation of hydration free-energies using macroscopic solvent models. *J Phys Chem*, **98**(7), 1978–1988 (1994).
45. H. Tjong, H. X. Zhou. Prediction of protein solubility from calculation of transfer free energy. *Biophys J*, **95**(6), 2601–2609 (2008).
46. Y. Shi, C. J. Wu, J. W. Ponder, P. Y. Ren. Multipole electrostatics in hydration free energy calculations. *J Computational Chem*, **32**(5), 967–977 (2011).
47. J. M. Wang, T. J. Hou. Recent advances on aqueous solubility prediction. *Combinatorial Chem & High Throughput Screening*, **14**(5), 328–338 (2011).
48. M. Manciu, E. Ruckenstein. The polarization model for hydration/double layer interactions: the role of the electrolyte ions. *Adv in Colloid Interface Science*, **112**(1–3), 109–128 (2004).

49. C. Azuara, H. Orland, M. Bon, P. Koehl, M. Delarue. Incorporating dipolar solvents with variable density in Poisson–Boltzmann electrostatics. *Biophys J*, **95**(12), 5587–5605 (2008).
50. K. A. T. Silverstein, A. D. J. Haymet, K. A. Dill. A simple model of water and the hydrophobic effect. *J Am Chem Soc*, **120**(13), 3166–3175 (1998).
51. S. Marcelja, N. Radic. Repulsion of interfaces due to boundary water. *Chem Phys Lett*, **42**(1), 129–130 (1976).
52. J. N. Israelachvili, H. Wennerstrom. Entropic forces between amphiphilic surfaces in liquids. *J Phys Chem*, **96**(2), 520–531 (1992).
53. E. S. Reiner, C. J. Radke. Variational approach to the electrostatic free-energy in charged colloidal suspensions: General theory for open systems. *J Chem Society, Faraday Transactions*, **86**(23), 3901–3912 (1990).
54. D. Andelman. Electrostatic properties of membranes: The Poisson–Boltzmann theory. In R. Lipowsky, E. Sackmann, (Eds.) *Structure and Dynamics of Membranes*, volume 1, second edition, section 12. Amsterdam: Elsevier, 603–642 (1995).
55. A. Kessel, B. Musafia, N. Ben-Tal. Continuum solvent model studies of the interactions of an anticonvulsant drug with a lipid bilayer. *Biophys J*, **80**(6), 2536–2545 (2001).
56. A. Ben-Shaul, I. Szleifer, W. M. Gelbart. Chain organization and thermodynamics in micelles and bilayers. i. theory. *J Chem Phys*, **83**, 3597–3611 (1985).
57. D. Harries, A. BenShaul. Conformational chain statistics in a model lipid bilayer: Comparison between mean field and Monte Carlo calculations. *J Chem Phys*, **106**(4), 1609–1619 (1997).
58. A. Zemel, A. Ben-Shaul, S. May. Membrane perturbation induced by interfacially adsorbed peptides. *Biophys J*, **86**(6), 3607–3619 (2004).
59. A. Fahr, P. Van Hoogevest, J. Kuntsche, M. L. S. Leigh. Lipophilic drug transfer between liposomal and biological membranes: What does it mean for parenteral and oral drug delivery? *J Liposome Research*, **16**(3), 281–301 (2006).
60. S. Balaz. Lipophilicity in trans-bilayer transport and subcellular pharmacokinetics. *Perspectives in Drug Discovery Design*, **19**(1), 157–177 (2000).
61. J. D. Jones, T. E. Thompson. Spontaneous phosphatidylcholine transfer by collision between vesicles at high lipid-concentration. *Biochemistry*, **28**(1), 129–134 (1989).
62. L. R. McLean, M. C. Phillips. Mechanism of cholesterol and phosphatidylcholine exchange or transfer between unilamellar vesicles. *Biochemistry*, **20**(10), 2893–2900 (1981).
63. S. Loew, A. Fahr, S. May. Modeling the release kinetics of poorly water-soluble drug molecules from liposomal nanocarriers. *J Drug Delivery*, **376548**(2011).
64. H. Hefesha, S. Loew, X. L. Liu, S. May, A. Fahr. Transfer mechanism of temoporfin between liposomal membranes. *J Controlled Release*, **150**(3), 279–286 (2011).
65. L. Masaro, X. X. Zhu. Physical models of diffusion for polymer solutions, gels and solids. *Progress in Polymer Science*, **24**(5), 731–775 (1999).
66. N. A. Peppas, A. R. Khare. Preparation, structure and diffusional behavior of hydrogels in controlled-release. *Adv Drug Delivery Rev*, **11**(1-2), 1–35 (1993).
67. S. Tenjarla. Microemulsions: An overview and pharmaceutical applications. *Critical Rev in Therapeutic Drug Carrier Systems*, **16**(5), 461–521 (1999).
68. V. Reshetov, D. Kachatkou, T. Shmigol, V. Zorin, M.A. D'Hallewin, F. Guillemin, L. Bezdetnaya. Redistribution of meta-tetra(hydroxyphenyl)chlorin (m-THPC) from

conventional and PEGylated liposomes to biological substrates. *Photochemical & Photobiological Sciences*, **10**(6), 911–919 (2011).

69. L. Zeng, L. An, X. Wu. Modeling drug-carrier interaction in the drug release from nanocarriers. *J Drug Delivery*, **370308**(2011).
70. C. Washington. Drug release from microparticulate systems (microencapsulations methods and industrial applications). In S. Benita, (Ed.) *Drugs and the Pharmaceutical Sciences 73*. New York: Marcel Dekker, 155–181 (1996).